

Invariance Principle Meets Out-of-Distribution Generalization on Graphs

Yongqiang Chen¹, Yonggang Zhang², Han Yang¹, Kaili Ma¹, Binghui Xie¹

¹The Chinese University of Hong Kong ²Hong Kong Baptist University
{yqchen,hyang,klma,bhxie21,jcheng}@cse.cuhk.edu.hk csyzhang@comp.hkbu.edu.hk

Tongliang Liu³, Bo Han^{2,1}, James Cheng¹

³University of Sydney
tongliang.liu@sydney.edu.au bhanml@comp.hkbu.edu.hk

Abstract

Despite recent developments in using the invariance principle from causality to enable out-of-distribution (OOD) generalization on Euclidean data, e.g., images, studies on graph data are limited. Different from images, the complex nature of graphs poses unique challenges that thwart the adoption of the invariance principle for OOD generalization. In particular, distribution shifts on graphs can happen at both structure-level and attribute-level, which increases the difficulty of capturing the invariance. Moreover, domain or environment partitions, which are often required by OOD methods developed on Euclidean data, can be expensive to obtain for graphs. Aiming to bridge this gap, we characterize distribution shifts on graphs with causal models, and show that the OOD generalization on graphs with invariance principle is possible by identifying an invariant subgraph for making predictions. We propose a novel framework to explicitly model this process using a contrastive strategy. By contrasting the estimated invariant subgraphs, our framework can provably identify the underlying invariant subgraph under mild assumptions. Experiments across several synthetic and real-world datasets demonstrate the state-of-the-art OOD generalization ability of our method.

1. Introduction

Graph representation learning with graph neural networks (GNNs) has gained huge success in tasks involving relational information (Kipf and Welling, 2017; Hamilton et al., 2017; Veličković et al., 2018; Xu et al., 2018, 2019). However, it assumes that the training and test data are drawn from the same distribution, which does not always hold in reality (Hu et al., 2020; Koh et al., 2021; Huang et al., 2021). The mismatch between training and test distribution, i.e., *distribution shifts*, introduced by some underlying environmental factors related to data collection or processing, can seriously degrade the performance of deployed models (Beery et al., 2018; DeGrave et al., 2021). Such *out-of-distribution* (OOD) generalization failures become the major roadblock for practical applications of graph representation learning models.

In parallel, enabling OOD generalization on Euclidean data has received surging attention and several solutions were proposed (Arjovsky et al., 2019; Sagawa* et al., 2020; Bengio et al., 2020; Gulrajani and Lopez-Paz, 2021; Schölkopf et al., 2021; Krueger et al., 2021; Creager et al., 2021; Ahuja et al., 2021). In particular, the invariance principle from causality is at the heart of those works (Peters et al., 2016; Pearl, 2009). The principle generically assumes that there exists a subset of inputs that carry most of the information about the underlying causes of the label. Predictions that merely focus on this part are invariant to a large class of distribution shifts in the sense of Independent Causal Mechanism (ICM) assumption (Pearl, 2009; Rojas-Carulla et al., 2018; Koyama and Yamaguchi, 2020; Ahuja et al., 2021).

Despite the success of the invariance principle on Euclidean data, the complex nature of graph data raises several unique challenges that prohibit direct applications of the principle. First, distribution

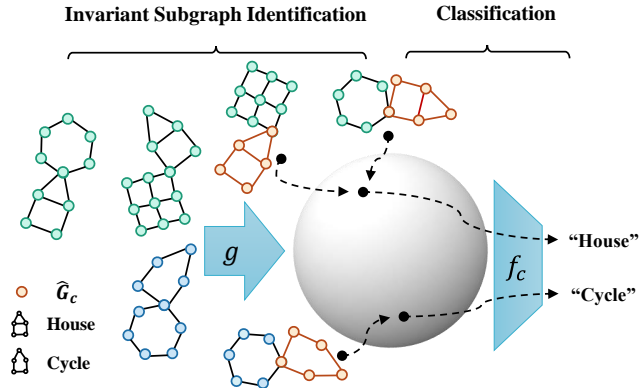


Figure 1: **Graph Out-Of-Distribution** generalization framework (GOOD): The featurizer g first identifies an (orange colored) invariant subgraph G_c for each input. The training of g employs a contrastive strategy so that the estimated G_c s will be mapped to a latent sphere with favorable properties for provable identifiability. With the identified invariant subgraph G_c , the predictions made by classifier f_c based on G_c are invariant to distribution shifts.

shifts on graphs can happen at both structure-level and attribute-level, and can exhibit via various graph properties such as graph sizes (Bevilacqua et al., 2021) and homophily (McPherson et al., 2001), which increases the difficulty of characterizing the sources of distribution shifts and capturing the invariance. Second, OOD algorithms developed and analyzed on Euclidean data often require additional environment (or domain) labels for distinguishing the sources of distribution shifts. However, collecting environment labels for graphs requires specific expert knowledge, which can be expensive due to the abstraction of graph data (Hu et al., 2020). Hence, the above problems pose the following problem:

How could we generalize the invariance principle to enable OOD generalization of GNNs?

In this paper, we provide answers to this question by studying the OOD generalization on graph classification. Specifically, we study 3 generic Structural Causal Models (SCM) (Pearl, 2009; Peters et al., 2017) for characterizing the graph generation process and distinguishing the sources of distribution shifts. Built upon these SCMs, we generalize the invariance principle to graphs. That is, when predicting the label for a specific graph G , we can identify an invariant and a critical subgraph G_c that contains and only contains most of the information in G about the underlying cause, so that the prediction for G based on G_c is stable to distribution shifts by the ICM assumption. Hence, the problem of achieving OOD generalization on graphs is rephrased into invariant subgraph identification and classification (Fig. 1).

To instantiate the invariance principle for graphs, we propose a novel framework, called **Graph Out-Of-Distribution** generalization (GOOD), to explicitly model the two sub-processes by decomposing a GNN model into the following two modules (cf., Fig. 1): a) a featurizer for identifying the underlying G_c from G ; b) a classifier for making predictions based on G_c . Specifically, the featurizer aims to distinguish the invariant subgraph G_c from the other parts of G that can be easily influenced by environment (or domain) shifts. A soft mask is applied to G for disentangling these two parts that are entangled at both structure and attribute level during the generation. To ensure the identifiability of the underlying G_c , we propose a contrastive strategy, inspired by the fact that the G_c s from the same classes should have high mutual information that is invariant to distribution shifts. We show that this strategy can enable the featurizer to provably identify the underlying G_c (Theorem 4.2). Therefore, the predictions that merely focus on the identified G_c are invariant to distribution shifts. We verify the

effectiveness of GOOD on several synthetic and real-world datasets with various distribution shifts. Our experiments demonstrate that GOOD significantly outperforms existing methods and achieves the state-of-the-art OOD generalization performance on graphs.

Our main contributions can be summarized as follows:

- Through the lens of causality, we establish general SCMs to characterize the distribution shifts on graphs, paving the way for generalizing the invariance principle to graphs (Sec. 3).
- We instantiate the invariance principle for OOD generalization on graphs through a novel framework GOOD, where the prediction is decomposed into the subgraph identification and classification. We show that the provable identifiability of the underlying invariant subgraph can be achieved using a contrastive strategy. Hence, the model can generalize to OOD graphs (Sec. 4).
- Extensive experiments on 13 synthetic and real-world datasets demonstrate that GOOD outperforms previous methods and achieves the state-of-the-art OOD generalization performance (Sec. 5).

2. Preliminaries

Graph Neural Networks. Let $G = (A, X)$ denote a graph with n nodes and m edges, where $A \in \{0, 1\}^{n \times n}$ is the adjacency matrix, and $X \in \mathbb{R}^{n \times d}$ is the node feature matrix with a node feature dimension of d . In graph classification, we are given a set of N graphs $\{G_i\}_{i=1}^N \subseteq \mathcal{G}$ and their labels $\{Y_i\}_{i=1}^N \subseteq \mathcal{Y} = \mathbb{R}^c$ from c classes. Then, we train a GNN $h_\theta \circ \rho$ with an encoder $h_\theta : \mathcal{G} \rightarrow \mathbb{R}^h$ that learns a meaningful representation r_G for each graph G to help predict their labels $y_G = \rho(r_G)$ with a downstream classifier $\rho : \mathbb{R}^h \rightarrow \mathcal{Y}$. The representation r_G is typically obtained by performing pooling with a READOUT function on the learned node representations:

$$r_G = \text{READOUT}(\{r_u^{(K)} | u \in V\}), \quad (1)$$

where the READOUT is a permutation invariant function (e.g., SUM, MEAN) (Ying et al., 2018; Murphy et al., 2019; Xu et al., 2019; Chen et al., 2020; Morris et al., 2021), and $r_u^{(K)}$ stands for the node representation of $u \in V$ at K -th layer that is obtained by neighbor aggregation:

$$r_u^{(K)} = \sigma(W_K \cdot a(\{r_v^{(K-1)}\}_{v \in \mathcal{N}(u) \cup \{u\}})), \quad (2)$$

where $\mathcal{N}(u)$ is the set of neighbors of node u , $\sigma(\cdot)$ is an activation function, e.g., ReLU, and $a(\cdot)$ is an aggregation function over neighbors, e.g., MEAN.

Invariant Learning and OOD generalization on graphs. Invariant learning typically considers a supervised learning setting based on the data $\mathcal{D} = \{\mathcal{D}^e\}_e$ collected from multiple environments \mathcal{E}_{all} , where $\mathcal{D}^e = \{G_i^e, y_i^e\}_{i=1}^{n^e}$ is the dataset from environment $e \in \mathcal{E}_{\text{all}}$, n^e is the number of instances in environment e , and $G_i^e \in \mathcal{G}$ and $y_i^e \in \mathcal{Y}$ correspond to the input graph and the label for the i -th instance from \mathcal{D}^e . (G_i^e, y_i^e) from a single environment e are considered as drawn independently from identical distribution \mathbb{P}^e . The goal of OOD generalization is to train a GNN $h_\theta \circ \rho : \mathcal{G} \rightarrow \mathcal{Y}$ with data from training environments $\mathcal{D}_{\text{tr}} = \{\mathcal{D}^e\}_{e \in \mathcal{E}_{\text{tr}} \subseteq \mathcal{E}_{\text{all}}}$, and generalize well to all (unseen) environments, i.e., to minimize:

$$\min_{\theta} \max_{e \in \mathcal{E}_{\text{all}}} R^e(h_\theta \circ \rho), \quad (3)$$

where R^e is the empirical risk under environment e (Vapnik, 1991; Peters et al., 2016; Arjovsky et al., 2019).

3. Graph OOD Generalization through the Lens of Causality

It is known that OOD generalization is impossible without assumptions on \mathcal{E}_{all} (Pearl, 2009; Ahuja et al., 2021). Thus, in this section, we first formulate the data generation process with structural causal

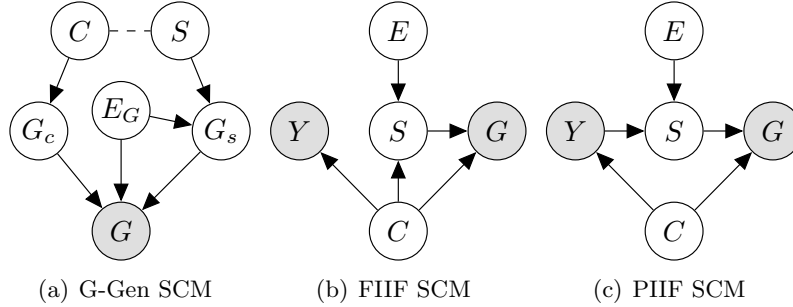


Figure 2: SCMs on graph distribution shifts.

model (SCM) and latent-variable model (Pearl, 2009; Peters et al., 2017; Kügelgen et al., 2021), and characterize the sources of distribution shifts on graphs. Then, we investigate whether the previous methods can be applied to achieving OOD generalization on graphs.

3.1 Graph generation process

We take a latent-variable model perspective on the graph generation and assume that the graph is generated through a mapping $f : \mathcal{Z} \rightarrow \mathcal{G}$, where $\mathcal{Z} \subseteq \mathbb{R}^n$ is the latent space and $\mathcal{G} = \cup_{N=1}^{\infty} \{0, 1\}^N \times \mathbb{R}^{N \times d}$ is the graph space. Following previous works (Kügelgen et al., 2021; Ahuja et al., 2021), we partition the latent variable into an invariant part $C \in \mathcal{C} = \mathbb{R}^{n_c}$ and a varying part $S \in \mathcal{S} = \mathbb{R}^{n_s}$, s.t., $n = n_c + n_s$. Let E be a random variable that denotes the environments. Given the partition of \mathcal{Z} , C keeps the invariant information that cannot be affected by E , while S keeps the varying information that can be affected by E ¹. C and S control the generation of the observed graphs (Assumption 3.1) and can have multiple types of interactions at the latent space (Assumption 3.2, 3.3).

Graph generation model. We formally elaborate the SCM for the graph generation process in Assumption 3.1 and Fig. 2(a), where noises in the structural equations are omitted for simplicity (Pearl, 2009; Peters et al., 2017).

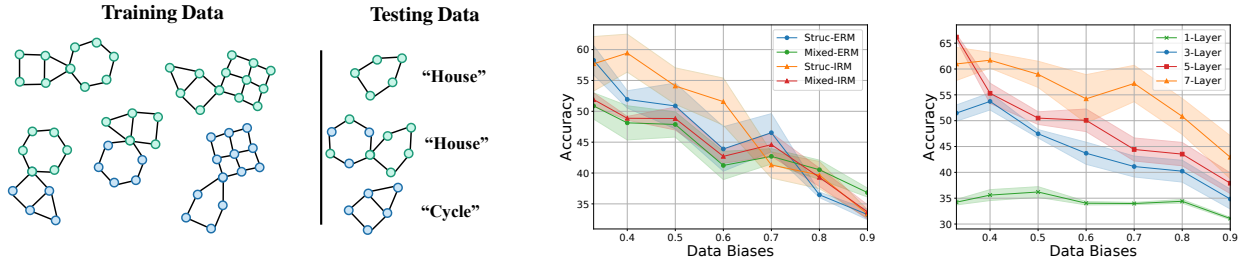
Assumption 3.1 (Graph Generation SCM).

$$\begin{aligned}
 (Z_A^c, Z_X^c) &:= f_{\text{gen}}^{(A,X)^c}(C), & (Z_A^s, Z_X^s) &:= f_{\text{gen}}^{(A,X)^s}(S), \\
 G_c &:= f_{\text{gen}}^{G_c}(Z_A^c, Z_X^c), & G_s &:= f_{\text{gen}}^{G_s}(Z_A^s, Z_X^s, E_G), \\
 G &:= f_{\text{gen}}^G(G_c, G_s, E_G).
 \end{aligned}$$

In Assumption 3.1, C and S control the generation of the adjacency matrices and features of the invariant subgraph G_c and spurious subgraph G_s through two pairs of latent variables (Z_A^c, Z_X^c) and (Z_A^s, Z_X^s) , respectively. Then, G_c and G_s are entangled into the observed graph G through f_{gen}^G . It can be a simply JOIN of a G_c with one or multiple G_s , or more complex generation processes controlled by the latent variables (Snijders and Nowicki, 1997; Lovász and Szegedy, 2006; You et al., 2018; Luo et al., 2021).

Moreover, a subset of environment latent variable $E_G \subseteq E$ will also affect the generation of G and G_s . Thus, graphs collected from different environments (or domains) can have different structure-level properties (e.g., degrees, graph sizes) (Bevilacqua et al., 2021) as well as feature-level properties (e.g., homophily) (Chen et al., 2022), while G_c remains invariant. In fact, the generation of many real-world

1. For images, C and S can be understood as content and style while E can be understood as locations the images are taken (Beery et al., 2018; Zhang et al., 2021; Kügelgen et al., 2021).



(a) Failure cases of GNN-ERM and GNN-IRM. (b) OOD failures of objectives. (c) OOD failures of deeper GNNs.

Figure 3: Failures of graph OOD generalization. (a) GNNs optimized with ERM (GNN-ERM) and IRM (GNN-IRM) are required to classify whether the graph contains a “house” or “cycle” motif, where the colors represent node features. However, distribution shifts in the training exists at both structure level (From left to right: “house” mostly co-occur with a hexagon), and at attribute level (From upper to lower: graphs nodes are mostly green colored if they contain “house”, or blue colored if they contain “cycle”). GNN-ERM tend to leverage these shortcuts and predict graphs that have a hexagon or have mostly green nodes as “house”. GNN-IRM tend to fail at testing data that is not covered by the training distribution. (b) Both GCNs with mean readout optimized with ERM and IRM cannot generalize to OOD, neither for structure-level shifts (Struc-) nor mixed with feature shifts (Mixed-). (c) GCNs with sum readout and more message passing layers are still sensitive to distribution shifts.

graphs can be abstracted as Assumption 3.1. For example, in drug discovery, the treatment effects of a drug to a specific disease is usually captured by a sub-molecule of the molecule graph, which is invariant across several species or domains (Bohacek et al., 1996; Sterling and Irwin, 2015).

Interactions at latent space. Depending on whether the latent invariant part C is fully informative about label Y , i.e., $(S, E) \perp Y|C$, the latent interactions between C and S can be categorized into Fully Informative Invariant Features (FIIF, Fig. 2(b)) and Partially Informative Invariant Features (PIIF, Fig. 2(c))². We follow Arjovsky et al. (2019); Ahuja et al. (2021) to formulate the SCMs for FIIF and PIIF with noises omitted for brevity (Pearl, 2009; Peters et al., 2017).

Assumption 3.2 (FIIF Structural Causal Model).

$$Y := f_{\text{inv}}(C), S := f_{\text{spu}}(C, E), G := f_{\text{gen}}(C, S).$$

Assumption 3.3 (PIIF Structural Causal Model).

$$Y := f_{\text{inv}}(C), S := f_{\text{spu}}(Y, E), G := f_{\text{gen}}(C, S).$$

In the two SCMs above, $f_{\text{gen}} : \mathcal{Z} = \mathbb{R}^{n_c+n_s} \rightarrow \mathcal{G}$ describes the graph generation process as Assumption 3.1. The generation of S is entailed by f_{spu} that takes E as one of the inputs. Besides, $f_{\text{inv}} : \mathcal{Z} = \mathbb{R}^{n_c} \rightarrow \mathcal{Y}$ separates and assigns labels for different C , which indicates the labelling process. For classification task, the separation assumption is usually necessary (Muller et al., 2001; Chen et al., 2005). Hence, we also introduce the following assumption on the separability for completeness, which are generically compatible with many other variants (Mika et al., 1999; Schölkopf, 2019).

2. Note that FIIF and PIIF can be mixed as Mixed Informative Invariant Features (Appendix 4(d)) in several ways, while our analysis will focus on the axiom ones for the purpose of generality.

Assumption 3.4 (Latent Separability). Given any pair of labels $(y, y') \sim \mathcal{Y} \times \mathcal{Y}$, the corresponding $(C, C') \sim J(y, y')$ are bounded³ and satisfy that:

$$\mathbb{E}_{C, C' \sim \mathcal{J}(y, y')} d(C, C') \leq \mathbb{E}_{C, C' \sim \mathcal{J}(y, y')} d(C, C'),$$

where $\mathcal{J}(y, y')$ is the joint conditional distribution $P_{C|Y=y, C'|Y=y'}$, $d(\cdot)$ is a distance measure at the latent space \mathcal{C} , and the equality holds if and only if $y = y'$.

3.2 Failures of graph OOD generalization

Built upon the setup of the graph generation process, in this section, we formally derive the concept of an invariant GNN that can generalize to OOD graphs. Then, we investigate whether the existing methods can endow GNNs with OOD generalization ability, i.e., learning an invariant GNN.

Definition 3.5 (Invariant GNN). Given a set of graphs with their labels $\mathcal{D} = \{G_i, y_i\}_{i=1}^N$ and environments \mathcal{E}_{all} that follow the same graph generation process in Sec. 3.1, considering a GNN $h_\theta \circ \rho$ that has a permutation invariant graph encoder $h_\theta : \mathcal{G} \rightarrow \mathbb{R}^h$ and a downstream classifier $\rho : \mathbb{R}^h \rightarrow \mathcal{Y}$, $h_\theta \circ \rho$ is an invariant GNN if it minimizes the worst risk at all environments, i.e., $\max_{e \in \mathcal{E}_{\text{all}}} R^e$ (Eq. 3).

With the above definition, we can analyze whether an invariant GNN can be learned with previous methods such as optimization objectives or architecture choices. We provide both theoretical discussions⁴ and empirical case studies based on the synthetic BAMotif (Luo et al., 2020) graphs shown in Fig. 3. Specific settings are given in Appendix C.

Can GNNs optimized with ERM generalize to OOD? Standard training of GNNs adopts the empirical risk minimization (ERM (Vapnik, 1991)) through minimizing the supervised losses over all training samples. However, neural networks optimized with ERM are shown to leverage the shortcuts, i.e., the parts in G that is strongly correlated with Y through S in a certain environment $E = e$, to make predictions (Geirhos et al., 2020). Hence, the predictions $P(Y|G, E = e)$ can be changed drastically when switching to another environment $E = e'$ such that $P(Y|G, E = e) \neq P(Y|G', E = e')$ even G and G' have the same label. In other words, predictors that rely on any subset of G controlled by S , can hardly generalize to OOD graphs, i.e., other environments. Considering a more concrete graph classification problem where all graphs contain only a single node, with strictly linear separable invariant features (i.e., f_{inv} is linear and f_{gen} is invertible⁵), there can be infinite Bayes optimal solutions (i.e., minimizers of the ERM objective), given limited coverage of all possible S at the training data. However, there only exists one invariant GNN predictor that merely focuses on the invariant features. Therefore, GNNs optimized with ERM will fail to generalize to OOD almost surely. Empirical results on more complex samples in Fig. 3(b) verified our conclusion.

Can message passing improve OOD generalization of GNNs? Aggregating neighbor information with more layers to denoise the input signal, or enhancing the expressivity with more powerful readout functions, are two common choices in GNNs to improve the generalization ability (Xu et al., 2018; Li et al., 2018; Xu et al., 2019; Yang et al., 2021). However, in Fig. 3(c), we empirically found that GCNs with more layers and more powerful sum readout are still sensitive to distribution shifts. In particular, stacking more layers can help denoise certain shifts, while the OOD performance will drop more sharply when the bias increases. Intuitively, if the spurious features from nodes cannot be eliminated by the denoising property of a deeper GNN, they can spread among the whole graph more widely, which in turn leads to stronger spurious correlations. Besides, the spurious correlations can be

3. We say C is bounded if $\exists 0 \leq M < \infty$ such that $\forall C, C' \in \mathcal{C}$, $d(C, C') \leq M$.

4. We provide formal failure cases in Appendix C.

5. More details are given in Appendix C.2.

more difficult to be disentangled if there are distribution shifts at both structure-level and attribute-level. Since the node representations from hidden layers can also encode graph topology features (Xu et al., 2019), distribution shifts introduced through Z_A^s and Z_X^s will doubly mix at the learned features. In the worst case, the information about Z_A^c and Z_X^c can be partially covered by or even replaced by Z_A^s and Z_X^s , which will greatly improve the difficulty or even make the OOD generalization impossible for message passing GNNs trained with ERM.

Can OOD objectives improve OOD generalization of GNNs? Recently, tackling the OOD generalization problem on Euclidean data with the invariance principle has obtained huge success (Peters et al., 2016; Arjovsky et al., 2019; Sagawa* et al., 2020; Krueger et al., 2021; Ahuja et al., 2021), where many objectives are proposed for regularizing the model behaviors. In the discussion, we focus on a representative objective, invariant risk minimization (IRM) (Arjovsky et al., 2019), while our discussion can also be extended for other similar objectives. Specifically, IRM formulates OOD generalization problem as:

$$\begin{aligned} \min_{\theta, f_c} \frac{1}{|\mathcal{E}_{\text{tr}}|} \sum_{e \in \mathcal{E}_{\text{tr}}} R^e(h_\theta \circ \rho) \\ \text{s.t. } \rho \in \arg \min_{\hat{\rho}} R^e(h_\theta \circ \hat{\rho}), \forall e \in \mathcal{E}_{\text{tr}}. \end{aligned}$$

Such formulation has promising theoretical properties for OOD generalization at linear regime that is also empirically verified on images (Arjovsky et al., 2019). However, there are two main issues that can degenerate the performance of IRM when applying to graphs. First, non-trivial environment partitions or labels are required for provably guarantees of optimality by IRM. However, collecting environment labels or meaning partitions of graphs requires expert knowledge and understandings about these abstract data structures, and thus they can be expensive to obtain and are usually not available in many benchmarks (Morris et al., 2020; Dwivedi et al., 2020; Hu et al., 2020). Alternative options for obtaining the partition such as random partitions, tend to give little help for graph OOD generalization (Creager et al., 2021), as it can be trivially deemed as mini-batching. Second, even with environment labels, IRM can hardly generalize to OOD or even fail catastrophically at non-linear regime if there is not sufficient support overlap with the test environments, i.e., $\cup_{e \in \mathcal{E}_{\text{te}}} \text{supp}(\mathbb{P}^e) \not\subseteq \cup_{e \in \mathcal{E}_{\text{tr}}} \text{supp}(\mathbb{P}^e)$ (Rosenfeld et al., 2021; Ahuja et al., 2021). In addition to IRM, the failure can also happen to other alternative objectives (Krueger et al., 2021; Bellot and van der Schaar, 2020; Ahuja et al., 2021) as stated in Theorem 5.1 in Rosenfeld et al. (2021).

3.3 Challenges of graph OOD generalization

The aforementioned failures reveal that existing OOD methods developed for Euclidean data can hardly be directly applied to graphs and pose new challenges for graph OOD generalization: a) Distribution shifts on graphs are more complicated as implied by Assumption. 3.1; b) Environment labels are usually not available due to the abstract graph data structure. Therefore, a natural question is raised: *Can we generalize and instantiate the invariance principle for OOD generalization on graphs?*

4. Invariance Principle for Graph OOD Generalization

We provide affirmative answers to the previous question. Built upon the SCMs established in Sec. 3.1, we generalize the invariance principle for graph OOD generalization, and propose a novel framework, **Graph Out Of Distribution** generalization (GOOD), to instantiate the principle with provable guarantees of OOD generalization ability.

4.1 Invariant subgraph for graph OOD generalization

Towards generalizing the invariance principle to graphs, observing that, for both FIIF and PIIF (Assumption 3.2, 3.3), the causal relationship $C \rightarrow Y$ is independent to environments E by the ICM assumption (Pearl, 2009; Peters et al., 2017). Furthermore, G_c carries the major information of C about Y in the observed graph G , hence the correlation between G_c and Y is also invariant across different environments. In other words, GNNs that merely focus on G_c to predict Y can generalize to OOD graphs.

Proposition 4.1. *Let \mathcal{G}_c denote the subgraph space for G_c , given a set of graphs with their labels $\mathcal{D} = \{G^{(i)}, y^{(i)}\}_{i=1}^N$ and \mathcal{E}_{all} that follow the graph generation process in Sec. 3.1, a GNN $h \circ \rho : \mathcal{G}_c \rightarrow \mathcal{Y}$ solving the following objective can generalize to OOD graphs in the sense of Definition. 3.5:*

$$\min_{\theta} R_{\mathcal{G}_c}(h_{\theta} \circ \rho),$$

where $R_{\mathcal{G}_c}$ is the empirical risk over $\{G_c^{(i)}, y^{(i)}\}_{i=1}^N$ and $G_c^{(i)}$ is the underlying invariant subgraph G_c for $G^{(i)}$.

Naturally, Proposition 4.1 paves a way towards graph OOD generalization, where an invariant predictions can be made via the following two sub-processes: a) Identifying the underlying invariant subgraph G_c ; b) Predicting the label for the original graph G based on G_c . Inspired by this observation, we propose the following implementation of Proposition 4.1 to learn an invariant GNN⁶ (Definition. 3.5):

$$\begin{aligned} \min_{\theta} R_{\hat{\mathcal{G}}_c}(h_{\theta} \circ \rho), \\ \text{s.t. } \hat{G}_c = \arg \max_{\tilde{G}_c \subseteq G} I(\tilde{G}_c; Y), Y \perp\!\!\!\perp E | \tilde{G}_c. \end{aligned} \quad (4)$$

4.2 GOOD Framework

The most difference of Eq. 4 from standard ERM is that, an invariant subgraph G_c needs to be isolated from G for making predictions, which is the key to achieve OOD generalization. However, identifying G_c can be difficult due to the complex entanglement of G_c and G_s in G as Assumption 3.1. Directly optimizing for such a complicated problem can hardly be realized without a proper architecture (Xu et al., 2020, 2021).

Inspired by the rationales of GNN reasoning uncovered by Xu et al. (2020), we propose the GOOD framework that *explicitly* aligns with the two sub-processes in Eq. 4, by decoupling the model into a featurizer and a classifier. Specifically, the featurizer $g : \mathcal{G} \rightarrow \mathcal{G}_c$ aims to identify the underlying G_c , and the classifier $f_c : \mathcal{G}_c \rightarrow \mathcal{Y}$ will predict the label Y based on the estimated G_c . Each input G will be processed as follows (see also Algorithm 1 in Appendix).

Featurizer. Instead of directly isolating a subgraph from G , the featurizer g predicts a *soft* subgraph \hat{G}_c by learning a soft mask M and applying it to obtain the $\hat{G}_c = M \odot G$, where \odot stands for the hadamard product. The output \hat{G}_c is a weighted graph for properly disentangling the complex mixing of the underlying G_c and G_s in Assumption 3.1.

Classifier. Given the estimated \hat{G}_c from the featurizer, the classifier f_c will predict the label $\hat{y} = f_c(\hat{G}_c)$. Once the underlying G_c is successfully disentangled, the predictions made by the classifier are invariant to distribution shifts introduced by E , in the sense of Proposition 4.1.

6. We denote the identification of G_c from G with a generalized \subseteq that takes subsets of edges and features from G or its projection into some feature space, i.e., $h_{\theta}(\mathcal{G})$.

Optimization objective. To train the model end-to-end, we merge $I(\hat{G}_c, Y)$ the empirical risk via the variational bound (Alemi et al., 2017; Yu et al., 2021):

$$I(\hat{G}_c, Y) \geq \int p(y, \hat{G}_c) \log p(y|\hat{G}_c) dy d\hat{G}_c \approx -R(\hat{G}_c, f_c), \quad (5)$$

hence we can further re-write Eq. 4 as:

$$\min_{g, f_c} R(\hat{G}_c, f_c), \text{ s.t. } Y \perp\!\!\!\perp E | \hat{G}_c, \hat{G}_c = g(G), \quad (6)$$

where $R(\hat{G}_c, f_c)$ is the empirical loss of f_c based on \hat{G}_c .

Eq. 6 provides a general approach to learn an invariant GNN. However, it is challenging to implement the independence constraint $Y \perp\!\!\!\perp E | \hat{G}_c$ into a differentiable objective, especially when the environment information E is unavailable. To mitigate this issue, we resort to utilize the properties of G_c implied by SCMs in Sec. 3.1. Specifically, given a set of graphs $\{G^{(i)}, y^{(i)}\}_{i=1}^N$, the underlying G_c s from the same class should have high mutual information across different environments. since causal relationship is stable to environment changes. In contrast, G_c and G_s do not have such properties as G_s is also affected by environment E .

Intuitively, if the size of the underlying G_c is known and fixed, i.e., $|G_c| = r_c$, we can get rid of potential G_s from the estimated \hat{G}_c by maximizing the mutual information between different \hat{G}_c s drawn from the same class. Hence, we can rephrase Eq. 6 as the following objective (GOODv1):

$$\max_{g, f_c} I(\hat{G}_c; Y) + I(\hat{G}_c; \tilde{G}_c | Y), \text{ s.t. } |g(G)| \leq r_c, \forall G, \quad (7)$$

where $\hat{G}_c = g(G)$, $\tilde{G}_c = g(\tilde{G})$ and $\tilde{G} \sim P(G|Y)$, i.e., \tilde{G} and G have the same label. However, the size of G_c is usually unknown or changes for different C . In this circumstance, maximizing Eq. 7 without constraints can lead to the presence of G_s in \hat{G}_c , causing predictions unstable to distribution shifts. For instance, $\hat{G}_c = G$ is a trivial solution to Eq. 7 when $r_c = \infty$.

To circumvent this limitation, we further resort to the properties of G_s . Intuitively, G_s or the left part after isolating \hat{G}_c from G , i.e., $G - \hat{G}_c$, should also have high mutual information between Y , for both FIIF and PIIF. Hence, we can enforce $G - \hat{G}_c$ to “compete” with \hat{G}_c when maximizing their mutual information between Y and them, respectively. Accordingly, we further derive GOODv2 as the following:

$$\begin{aligned} \max_{g, f_c} & I(\hat{G}_c; Y) + I(\hat{G}_c; \tilde{G}_c | Y) + I(\hat{G}_s; Y), \\ \text{s.t.} & I(\hat{G}_s; Y) \leq I(\hat{G}_c; Y), \hat{G}_s = G - \hat{G}_c, \end{aligned} \quad (8)$$

where (\hat{G}_c, \tilde{G}) are the same as Eq. 7.

4.3 Theoretical Analysis and Practical Discussions

We derive theoretical guarantees to show how objectives Eq. 7 and Eq. 8 can help identify the underlying G_c . Then, we introduce the practical implementations for Eq. 7 and Eq. 8, as well as further implications of our theory.

Theorem 4.2 (GOOD Induces Invariant GNN). *Given a set of graphs with their labels $\mathcal{D} = \{G^{(i)}, y^{(i)}\}_{i=1}^N$ and \mathcal{E}_{all} that follow the graph generation process in Sec. 3.1 with invertible f_{gen}^c and noises set U s.t. $H(U) \rightarrow 0$, assuming that the samples from each training environments with $|\mathcal{E}_{tr}| \geq 2$ are equally distributed, considering a model $g \circ f_c$ induced by GOOD embedded with sufficient expressive permutation invariant encoders $h : \mathcal{G}_c \rightarrow \mathbb{R}^h$ that can differentiate every graph in the support of all environments $\cup_{G^e \in \cup_{e \in \mathcal{E}_{all}} \text{supp}(\mathbb{P}^e)} \mathcal{P}(G^e)$ where $\mathcal{P}(G^e)$ is the power set of G^e :*

- (i) if $|G_c| = r_c$, $\forall G$ is known, and the size of the estimated subgraph is constrained $\hat{G}_c = g(G) \leq r_c, \forall G$, then each solution $g \circ f_c$ to Eq. 7, elicits an invariant GNN (Definition. 3.5) in the sense of Proposition 4.1.
- (ii) each solution $g \circ f_c$ to Eq. 8, elicits an invariant GNN (Definition. 3.5) in the sense of Proposition 4.1.

We prove Theorem 4.2 (i) and (ii) in Appendix D.2, D.3, respectively. Intuitively, merely maximizing the mutual information between Y and \hat{G}_c is essentially performing ERM that may introduce spurious subsets $G_s^p \subseteq G_s$ into \hat{G}_c . In contrast, simultaneously maximizing $I(\hat{G}_c; \tilde{G}_c|Y)$ with the competition constraint can serve as a regularization that prunes those redundant G_s^p .

Practical implementations of GOOD objectives. After showing the power of GOOD, we introduce the practical implementations of GOODv1 and GOODv2 objectives. The approximation of the first term $I(\hat{G}_c; Y)$ can be achieved via the variational bound as Eq. 5. While the exact estimation of the second term $I(\hat{G}_c; \tilde{G}_c|Y)$ can be expensive, contrastive learning provides a practical solution for its approximation (Chopra et al., 2005; Salakhutdinov and Hinton, 2007; van den Oord et al., 2018; Belghazi et al., 2018):

$$I(\hat{G}_c; \tilde{G}_c|Y) \approx \mathbb{E}_{\substack{(\hat{G}, \tilde{G}) \sim \mathcal{P}(\hat{G}, \tilde{G}|y) \\ \{G^i\}_{i=1}^M \sim \mathcal{P}(G|Y|y)}}} \sigma(\hat{G}, \tilde{G}, \{G^i\}_{i=1}^M), \quad (9)$$

where $\sigma(\hat{G}, \tilde{G}, \{G^i\}_{i=1}^M)$ is defined as:

$$\sigma(\hat{G}, \tilde{G}, \{G^i\}_{i=1}^M) = \log \frac{e^{\phi(h_{\hat{G}_c}, h_{\tilde{G}_c})}}{e^{\phi(h_{\hat{G}_c}, h_{\tilde{G}_c})} + \sum_i^M e^{\phi(h_{\hat{G}_c}^T, h_{G_c^i})}},$$

where ϕ represents a similarity metric, e.g. cosine similarity, and $\hat{G}_c = g(\hat{G}), \tilde{G}_c = g(\tilde{G}), G_c^i = g(G^i)$. As $|M| \rightarrow \infty$, Eq. 9 approximates $I(\hat{G}_c; \tilde{G}_c|Y)$ in the sense of non-parametric resubstitution entropy estimator via von Mises-Fisher kernel density estimation (Ahmad and Lin, 1976; Kandasamy et al., 2015; Wang and Isola, 2020). Hence, plugging it into Eq. 7, 8 can relieve the issue when approximating $I(\hat{G}_c; \tilde{G}_c|Y)$ in practice.

As for the third term $I(\hat{G}_s; Y)$ and the constraint $I(\hat{G}_s; Y) \leq I(\hat{G}_c; Y)$, a practical implementation is to follow the idea of hinge loss:

$$I(\hat{G}_s; Y) \sim \frac{1}{N} R_{\hat{G}_s} \cdot \mathbb{I}(R_{\hat{G}_s} \leq R_{\hat{G}_c}), \quad (10)$$

where N is the number of samples, \mathbb{I} is an indicator function that outputs 1 when the interior condition is satisfied otherwise 0, and $R_{\hat{G}_s}$ and $R_{\hat{G}_c}$ are the empirical risk vector of the predictions for each sample based on G_s and G_c respectively. We leave more details about our implementation in the experiments in Appendix E.2.

Significance and implications of GOOD. Although primarily serving for graph OOD generalization problem, our theory complements the identifiability study on graphs through contrastive learning, and aligns with the discoveries in the image domain that contrastive learning learns to isolate the content (C) and style (S) (Zimmermann et al., 2021; Kügelgen et al., 2021). Moreover, our theoretical analysis also partially explains the empirical success of graph contrastive learning (You et al., 2020; Ma et al., 2021; You et al., 2021), where the GNN may implicitly learn to identify the underlying invariant subgraph. Besides, the framework of GOOD can also be applied to other tasks involving relational information such as node classification. Thorough discussions and more details are given in Appendix A.

Table 1: OOD generalization performance on structure and mixed shifts in synthetic graphs in terms of accuracy.

	SPMOTIF-STRUC						SPMOTIF-MIXED					
	BIAS=0.33		BIAS=0.60		BIAS=0.90		BIAS=0.33		BIAS=0.60		BIAS=0.90	
	TEST (↑)	TRAIN	TEST (↑)	TRAIN	TEST (↑)	TRAIN	TEST (↑)	TRAIN	TEST (↑)	TRAIN	TEST (↑)	TRAIN
ERM	59.49 (3.50)	99.67 (0.08)	55.48 (4.84)	99.54 (0.07)	49.64 (4.63)	99.05 (0.79)	58.18 (4.30)	99.24 (0.31)	49.23 (4.22)	98.60 (0.42)	41.36 (3.29)	99.23 (0.38)
ASAP	56.21 (3.72)	99.57 (0.20)	55.11 (4.82)	99.33 (0.53)	47.30 (6.08)	99.59 (0.19)	55.21 (3.99)	98.47 (1.63)	52.56 (3.24)	99.05 (0.57)	41.05 (1.48)	99.45 (0.13)
DIR	59.58 (5.62)	98.53 (1.02)	59.18 (6.52)	96.22 (1.79)	47.03 (13.6)	90.22 (15.2)	67.28 (4.06)	96.70 (1.44)	58.93 (14.3)	91.07 (12.2)	38.58 (5.88)	74.14 (22.7)
IRM	60.37 (8.93)	99.57 (0.20)	54.99 (4.89)	99.39 (0.33)	53.70 (6.50)	99.61 (0.11)	58.03 (3.54)	99.04 (0.48)	49.79 (4.84)	98.38 (0.92)	41.38 (2.35)	99.51 (0.20)
V-REX	49.91 (3.33)	98.22 (0.98)	48.87 (1.68)	98.24 (1.17)	48.60 (4.93)	97.99 (0.81)	50.10 (1.45)	98.78 (0.42)	47.81 (2.90)	98.51 (0.72)	48.04 (2.31)	98.19 (0.77)
EIIL	57.11 (4.96)	99.58 (0.11)	54.01 (5.62)	98.98 (0.96)	49.79 (11.6)	99.52 (0.39)	54.29 (4.83)	98.57 (0.70)	49.02 (3.63)	98.80 (0.54)	41.30 (2.05)	99.27 (0.19)
IB-IRM	56.53 (3.30)	99.61 (0.19)	53.03 (5.35)	99.07 (0.38)	43.94 (2.02)	99.35 (0.29)	59.67 (4.49)	98.83 (1.16)	52.47 (6.98)	97.68 (1.94)	38.34 (2.00)	99.32 (0.40)
GOODv1	64.84 (9.21)	99.40 (1.17)	62.23 (9.13)	99.56 (0.27)	54.03 (6.92)	98.07 (2.55)	67.50 (4.99)	99.81 (0.16)	66.77 (11.6)	99.45 (0.38)	45.11 (9.58)	97.36 (2.83)
GOODv2	64.75 (9.40)	96.69 (7.12)	74.76 (13.1)	99.82 (0.17)	59.06 (10.7)	98.83 (1.48)	66.82 (13.9)	93.63 (11.4)	65.33 (9.84)	96.82 (5.48)	51.60 (7.30)	98.80 (0.70)

5. Experiments

We conduct extensive experiments with 13 datasets including both synthetic data and real-world data that have various distribution shifts, to comprehensively verify our theoretical findings and the effectiveness of GOOD. We leave more details about our experimental setup in Appendix E due to space constraint.

Datasets. According to graph generation process in Sec. 3.1, we use BAMotif (Ying et al., 2019; Luo et al., 2020; Wu et al., 2022b) to construct 3-class SPMotif datasets with artificial FIIF distribution shifts at the structural level (SPMotif-Struc), and a more difficult version mixed with FIIF distribution shifts at attribute level (SPMotif-Mixed). We also use four of TU datasets (Morris et al., 2020) to with distribution shifts at graph sizes (Yehudai et al., 2021; Bevilacqua et al., 2021). Meanwhile, we convert the colored mnist dataset in IRM (Arjovsky et al., 2019) using the same algorithm as Knyazev et al. (2019), and also split Graph-SST (Yuan et al., 2020) to inject degree biases, to cover more types of distribution shifts that possibly appear in graphs. More details about the datasets can be found in Appendix E.1.

Baselines and our methods. In terms of optimization objectives, we compare GOOD to the state-of-the-art OOD objectives including IRM (Arjovsky et al., 2019), v-Rex (Krueger et al., 2021) and IB-IRM (Ahuja et al., 2021), where we generate random environment partitions for these methods. Besides, we also compare GOOD with the only OOD objective EIIL (Creager et al., 2021) that does not require environment information. In terms of architectures, we compare our methods to the state-of-the-art interpretable GNN methods GIB (Yu et al., 2021), ASAP Pooling (Ranjan et al., 2020), and DIR (Wu et al., 2022b) that enables OOD GNN explainability. We select the interpretability ratio (i.e., r_c) according to the validation performances for both GNN explainability baselines and GOOD. We use a 3-layer GNN encoder for all methods for fair comparison. More implementation details are given in Appendix E.4.

Evaluation. We report classification accuracy for all datasets by default, except for TU datasets where we use Matthews correlation coefficient following the previous work (Bevilacqua et al., 2021). We repeat the evaluation multiple times, select model based on its performance at the validation set during each run, and report the mean and standard deviation of the corresponding metric.

OOD generalization performance on structure and mixed shifts. In Table 1, we report the training accuracy and testing accuracy of each method, whereas we omit GIB due to its consistent divergence. Different biases indicate different levels of distribution shifts. First, it can be found that most of the methods converge to more than 99% training accuracy, while the test accuracy decreases dramatically as the bias increases and as the distribution shifts are mixed, concluding our discussions in Sec. 3.2. Moreover, since G_c and G_s in the test data have appeared during training, OOD objectives or even interpretable baselines without specialized design for OOD generalization can improve the test accuracy in a certain level. However, GOODv1 outperforms most previous methods up to 10% and

Table 2: OOD generalization performance on graph size shifts in real-world graphs in terms of Matthews correlation coefficient.

Datasets	NCI1	NCI109	PROTEINS	DD	Avg
ERM	0.15 (0.05)	0.16 (0.02)	0.22 (0.09)	0.27 (0.09)	0.20
ASAP	0.14 (0.10)	0.15 (0.09)	0.15 (0.19)	0.22 (0.13)	0.17
GIB	0.13 (0.10)	0.16 (0.02)	0.19 (0.08)	0.01 (0.18)	0.12
DIR	0.21 (0.06)	0.13 (0.05)	0.25 (0.14)	0.20 (0.10)	0.20
IRM	0.17 (0.02)	0.14 (0.01)	0.21 (0.09)	0.22 (0.08)	0.19
V-REX	0.15 (0.04)	0.15 (0.04)	0.22 (0.06)	0.21 (0.07)	0.18
EIIL	0.14 (0.03)	0.16 (0.02)	0.20 (0.05)	0.23 (0.10)	0.19
IB-IRM	0.15 (0.06)	0.14 (0.04)	0.23 (0.05)	0.19 (0.13)	0.18
WL KERNEL	0.39 (0.00)	0.21 (0.00)	0.00 (0.00)	0.00 (0.00)	0.15
GC KERNEL	0.02 (0.00)	0.00 (0.00)	0.29 (0.00)	0.00 (0.00)	0.08
$\Gamma_{\text{I-HOT}}$	0.17 (0.08)	0.25 (0.06)	0.12 (0.09)	0.23 (0.08)	0.19
Γ_{GIN}	0.24 (0.04)	0.18 (0.04)	0.29 (0.11)	0.28 (0.06)	0.25
Γ_{RPGIN}	0.26 (0.05)	0.20 (0.04)	0.25 (0.12)	0.20 (0.05)	0.23
GOODv1	0.22 (0.07)	0.23 (0.09)	0.40 (0.06)	0.29 (0.08)	0.29
GOODv2	0.27 (0.07)	0.22 (0.05)	0.31 (0.12)	0.26 (0.08)	0.27

Table 3: OOD generalization performance on other distribution shifts in real-world graphs in terms of accuracy.

Datasets	CMnist-sp	Graph-SST5	Twitter	Avg
ERM	13.96 (5.48)	43.89 (1.73)	60.81 (2.05)	39.56
ASAP	10.79 (1.44)	44.67 (1.31)	62.36 (1.40)	39.27
GIB	15.40 (3.91)	38.64 (4.52)	48.08 (2.27)	34.04
DIR	15.50 (8.65)	41.12 (1.96)	59.85 (2.98)	38.82
IRM	10.80 (0.83)	43.69 (1.26)	63.50 (1.23)	39.33
V-REX	11.20 (1.07)	43.28 (0.52)	63.21 (1.57)	39.23
EIIL	10.30 (0.37)	42.98 (1.03)	62.76 (1.72)	38.68
IB-IRM	14.43 (1.04)	43.11 (1.75)	62.20 (1.59)	39.91
GOODv1	19.77 (17.1)	44.71 (1.14)	63.66 (0.84)	42.71
GOODv2	36.42 (11.5)	45.25 (1.27)	64.45 (1.99)	48.71

GOODv2 further pushes the state-of-the-art further up to 12%, which verifies the effectiveness of GOOD.

OOD generalization performance on graph size shifts. In Table 2, we additionally compare GOOD to the specialized designed methods for OOD generalization in terms of graph sizes (Γ GNNs) (Bevilacqua et al., 2021), where we include the author reported results for both kernel methods and Γ GNNs. It can be found that GOOD consistently and significantly outperforms the previous state-of-the-art, which further demonstrates the generality of GOOD.

OOD generalization performance on other shifts. In Table 3, we experiment with more types of distribution shifts that can appear on graphs. Notably, since the underlying generation processes of these datasets are more complex, the ground truth ratio r_c may not be fixed. Hence, the superiority of GOODv1 can be degraded when compared to other baselines, while GOODv2 keeps its outstanding OOD generalization ability that outperforms all of the other methods by a significant margin, serving for a strong evidence for our theoretical conclusion and its effectiveness.

6. Conclusion

We studied the OOD generalization problem in graph classification. Through the lens of causality, we established SCMs for characterizing the distribution shifts that can happen on graphs, generalized and instantiated the invariance principle to graphs via a novel framework GOOD that has promising theoretical and empirical OOD generalization ability.

References

- I. Ahmad and Pi-Erh Lin. A nonparametric estimation of the entropy for absolutely continuous distributions (corresp.). *IEEE Transactions on Information Theory*, 22(3):372–375, 1976.
- Kartik Ahuja, Ethan Caballero, Dinghuai Zhang, Jean-Christophe Gagnon-Audet, Yoshua Bengio, Ioannis Mitliagkas, and Irina Rish. Invariance principle meets information bottleneck for out-of-distribution generalization. In *Advances in Neural Information Processing Systems*, 2021.
- Alexander A. Alemi, Ian Fischer, and Joshua V. Dillon and. Deep variational information bottleneck. In *International Conference on Learning Representations*, 2017.
- Martín Arjovsky, Léon Bottou, Ishaan Gulrajani, and David Lopez-Paz. Invariant risk minimization. *arXiv preprint*, arXiv:1907.02893, 2019.

- Peter W. Battaglia, Razvan Pascanu, Matthew Lai, Danilo Jimenez Rezende, and Koray Kavukcuoglu. Interaction networks for learning about objects, relations and physics. In *Advances in Neural Information Processing Systems*, pages 4502–4510, 2016.
- Sara Beery, Grant Van Horn, and Pietro Perona. Recognition in terra incognita. In *Computer Vision European Conference, Part XVI*, volume 11220, pages 472–489, 2018.
- Mohamed Ishmael Belghazi, Aristide Baratin, Sai Rajeshwar, Sherjil Ozair, Yoshua Bengio, Aaron Courville, and Devon Hjelm. Mutual information neural estimation. In *International Conference on Machine Learning*, volume 80, pages 531–540, 10–15 Jul 2018.
- Alexis Bellot and Mihaela van der Schaar. Generalization and invariances in the presence of unobserved confounding. *arXiv preprint*, arXiv:2007.10653, 2020.
- Yoshua Bengio, Tristan Deleu, Nasim Rahaman, Nan Rosemary Ke, Sébastien Lachapelle, Olexa Bilaniuk, Anirudh Goyal, and Christopher J. Pal. A meta-transfer objective for learning to disentangle causal mechanisms. In *International Conference on Learning Representations*, 2020.
- Beatrice Bevilacqua, Yangze Zhou, and Bruno Ribeiro. Size-invariant graph representations for graph classification extrapolations. In *International Conference on Machine Learning*, volume 139, pages 837–851, 18–24 Jul 2021.
- Regine S. Bohacek, Colin McMartin, and Wayne C. Guida. The art and practice of structure-based drug design: A molecular modeling perspective. *Medicinal Research Reviews*, 16(1):3–50, 1996.
- Shiyu Chang, Yang Zhang, Mo Yu, and Tommi S. Jaakkola. Invariant rationalization. In *International Conference on Machine Learning*, volume 119, pages 1448–1458, 2020.
- Pai-Hsuen Chen, Chih-Jen Lin, and Bernhard Schölkopf. A tutorial on ν -support vector machines. *Applied Stochastic Models in Business and Industry*, 21(2):111–136, 2005.
- Yongqiang Chen, Han Yang, Yonggang Zhang, Kaili Ma, Tongliang Liu, Bo Han, and James Cheng. Understanding and improving graph injection attack by promoting unnoticeability. In *International Conference on Learning Representations*, 2022.
- Zhengdao Chen, Lei Chen, Soledad Villar, and Joan Bruna. Can graph neural networks count substructures? In *Advances in Neural Information Processing Systems*, 2020.
- Sumit Chopra, Raia Hadsell, and Yann LeCun. Learning a similarity metric discriminatively, with application to face verification. In *2005 IEEE Computer Society Conference on Computer Vision and Pattern Recognition (CVPR 2005), 20-26 June 2005, San Diego, CA, USA*, pages 539–546, 2005.
- Ching-Yao Chuang, Antonio Torralba, and Stefanie Jegelka. Estimating generalization under distribution shifts via domain-invariant representations. In *International Conference on Machine Learning*, volume 119, pages 1984–1994. PMLR, 2020.
- Thomas M. Cover and Joy A. Thomas. *Elements of Information Theory (Wiley Series in Telecommunications and Signal Processing)*. Wiley-Interscience, USA, 2006. ISBN 0471241954.
- Elliot Creager, Jörn-Henrik Jacobsen, and Richard S. Zemel. Environment inference for invariant learning. In *International Conference on Machine Learning*, volume 139, pages 2189–2200, 2021.

- Alex J. DeGrave, Joseph D. Janizek, and Su-In Lee. AI for radiographic COVID-19 detection selects shortcuts over signal. *Nature Machine Intelligence*, 3(7):610–619, 2021.
- Jacob Devlin, Ming-Wei Chang, Kenton Lee, and Kristina Toutanova. BERT: Pre-training of deep bidirectional transformers for language understanding. In *Conference of the North American Chapter of the Association for Computational Linguistics: Human Language Technologies, Volume 1 (Long and Short Papers)*, pages 4171–4186, 2019.
- Li Dong, Furu Wei, Chuanqi Tan, Duyu Tang, Ming Zhou, and Ke Xu. Adaptive recursive neural network for target-dependent twitter sentiment classification. In *Annual Meeting of the Association for Computational Linguistics*, pages 49–54, 2014.
- Vijay Prakash Dwivedi, Chaitanya K Joshi, Thomas Laurent, Yoshua Bengio, and Xavier Bresson. Benchmarking graph neural networks. *arXiv preprint*, arXiv:2003.00982, 2020.
- Matthias Fey and Jan E. Lenssen. Fast graph representation learning with PyTorch Geometric. In *ICLR Workshop on Representation Learning on Graphs and Manifolds*, 2019.
- Matt Gardner, Joel Grus, Mark Neumann, Oyvind Tafjord, Pradeep Dasigi, Nelson F. Liu, Matthew E. Peters, Michael Schmitz, and Luke Zettlemoyer. Allennlp: A deep semantic natural language processing platform. *arXiv preprint*, arXiv:1803.07640, 2018.
- Robert Geirhos, Jörn-Henrik Jacobsen, Claudio Michaelis, Richard S. Zemel, Wieland Brendel, Matthias Bethge, and Felix A. Wichmann. Shortcut learning in deep neural networks. *Nat. Mach. Intell.*, 2(11):665–673, 2020.
- Ishaan Gulrajani and David Lopez-Paz. In search of lost domain generalization. In *International Conference on Learning Representations*, 2021.
- William L. Hamilton, Zitao Ying, and Jure Leskovec. Inductive representation learning on large graphs. In *Advances in Neural Information Processing Systems*, pages 1024–1034, 2017.
- Kehang Han, Balaji Lakshminarayanan, and Jeremiah Zhe Liu. Reliable graph neural networks for drug discovery under distributional shift. In *NeurIPS 2021 Workshop on Distribution Shifts: Connecting Methods and Applications*, 2021.
- Weihua Hu, Matthias Fey, Marinka Zitnik, Yuxiao Dong, Hongyu Ren, Bowen Liu, Michele Catasta, and Jure Leskovec. Open graph benchmark: Datasets for machine learning on graphs. In *Advances in Neural Information Processing Systems*, 2020.
- Kexin Huang, Tianfan Fu, Wenhao Gao, Yue Zhao, Yusuf H Roohani, Jure Leskovec, Connor W. Coley, Cao Xiao, Jimeng Sun, and Marinka Zitnik. Therapeutics data commons: Machine learning datasets and tasks for drug discovery and development. In *Advances in Neural Information Processing Systems Datasets and Benchmarks Track (Round 1)*, 2021.
- Sergey Ioffe and Christian Szegedy. Batch normalization: Accelerating deep network training by reducing internal covariate shift. In *International Conference on Machine Learning*, volume 37, pages 448–456, 2015.
- Kirthevasan Kandasamy, Akshay Krishnamurthy, Barnabas Poczos, Larry Wasserman, and James M. Robins. Nonparametric von mises estimators for entropies, divergences and mutual informations. In *Advances in Neural Information Processing Systems*, volume 28, 2015.

- Prannay Khosla, Piotr Teterwak, Chen Wang, Aaron Sarna, Yonglong Tian, Phillip Isola, Aaron Maschinot, Ce Liu, and Dilip Krishnan. Supervised contrastive learning. In *Advances in Neural Information Processing Systems*, volume 33, pages 18661–18673, 2020.
- Diederik P. Kingma and Jimmy Ba. Adam: A method for stochastic optimization. In *International Conference on Learning Representations*, 2015.
- Thomas N. Kipf and Max Welling. Variational graph auto-encoders. *arXiv preprint*, arXiv:1611.07308, 2016.
- Thomas N. Kipf and Max Welling. Semi-supervised classification with graph convolutional networks. In *International Conference on Learning Representations*, 2017.
- Boris Knyazev, Graham W. Taylor, and Mohamed R. Amer. Understanding attention and generalization in graph neural networks. In *Advances in Neural Information Processing Systems*, pages 4204–4214, 2019.
- Pang Wei Koh, Shiori Sagawa, Henrik Marklund, Sang Michael Xie, Marvin Zhang, Akshay Balsubramani, Weihua Hu, Michihiro Yasunaga, Richard Lanus Phillips, Irena Gao, Tony Lee, Etienne David, Ian Stavness, Wei Guo, Berton Earnshaw, Imran Haque, Sara M. Beery, Jure Leskovec, Anshul Kundaje, Emma Pierson, Sergey Levine, Chelsea Finn, and Percy Liang. WILDS: A benchmark of in-the-wild distribution shifts. In *International Conference on Machine Learning*, volume 139, pages 5637–5664, 2021.
- Masanori Koyama and Shoichiro Yamaguchi. Out-of-distribution generalization with maximal invariant predictor. *arXiv preprint*, arXiv:2008.01883, 2020.
- David Krueger, Ethan Caballero, Jörn-Henrik Jacobsen, Amy Zhang, Jonathan Binas, Dinghui Zhang, Rémi Le Priol, and Aaron C. Courville. Out-of-distribution generalization via risk extrapolation (rex). In *International Conference on Machine Learning*, volume 139, pages 5815–5826, 2021.
- Julius Von Kügelgen, Yash Sharma, Luigi Gresele, Wieland Brendel, Bernhard Schölkopf, Michel Besserve, and Francesco Locatello. Self-supervised learning with data augmentations provably isolates content from style. In *Advances in Neural Information Processing Systems*, 2021.
- Qimai Li, Zhichao Han, and Xiao-Ming Wu. Deeper insights into graph convolutional networks for semi-supervised learning. In *AAAI Conference on Artificial Intelligence*, pages 3538–3545, 2018.
- Wanyu Lin, Hao Lan, and Baochun Li. Generative causal explanations for graph neural networks. In *International Conference on Machine Learning*, volume 139, pages 6666–6679, 2021.
- László Lovász and Balázs Szegedy. Limits of dense graph sequences. *Journal of Combinatorial Theory, Series B*, 96(6):933–957, 2006.
- Dongsheng Luo, Wei Cheng, Dongkuan Xu, Wenchao Yu, Bo Zong, Haifeng Chen, and Xiang Zhang. Parameterized explainer for graph neural network. In *Advances in Neural Information Processing Systems*, 2020.
- Youzhi Luo, Keqiang Yan, and Shuiwang Ji. Graphdf: A discrete flow model for molecular graph generation. In *International Conference on Machine Learning*, volume 139, pages 7192–7203, 2021.
- Kaili Ma, Haochen Yang, Han Yang, Tatiana Jin, Pengfei Chen, Yongqiang Chen, Barakeel Fansou Kamhoua, and James Cheng. Improving graph representation learning by contrastive regularization. *arXiv preprint*, arXiv:2101.11525, 2021.

- Miller McPherson, Lynn Smith-Lovin, and James M Cook. Birds of a feather: Homophily in social networks. *Annual Review of Sociology*, 27(1):415–444, 2001.
- Sebastian Mika, Gunnar Ratsch, Jason Weston, Bernhard Scholkopf, and Klaus-Robert Mullers. Fisher discriminant analysis with kernels. In *Neural networks for signal processing IX: Proceedings of the 1999 IEEE signal processing society workshop (cat. no. 98th8468)*, pages 41–48, 1999.
- Christopher Morris, Nils M. Kriege, Franka Bause, Kristian Kersting, Petra Mutzel, and Marion Neumann. Tudataset: A collection of benchmark datasets for learning with graphs. *arXiv preprint*, arXiv:2007.08663, 2020.
- Christopher Morris, Yaron Lipman, Haggai Maron, Bastian Rieck, Nils M. Kriege, Martin Grohe, Matthias Fey, and Karsten M. Borgwardt. Weisfeiler and leman go machine learning: The story so far. *arXiv preprint*, arXiv:2112.09992, 2021.
- K-R Muller, Sebastian Mika, Gunnar Ratsch, Koji Tsuda, and Bernhard Scholkopf. An introduction to kernel-based learning algorithms. *IEEE transactions on neural networks*, 12(2):181–201, 2001.
- Ryan L. Murphy, Balasubramaniam Srinivasan, Vinayak A. Rao, and Bruno Ribeiro. Relational pooling for graph representations. In *International Conference on Machine Learning*, volume 97, pages 4663–4673, 2019.
- Adam Paszke, Sam Gross, Francisco Massa, Adam Lerer, James Bradbury, Gregory Chanan, Trevor Killeen, Zeming Lin, Natalia Gimelshein, Luca Antiga, Alban Desmaison, Andreas Kopf, Edward Yang, Zachary DeVito, Martin Raison, Alykhan Tejani, Sasank Chilamkurthy, Benoit Steiner, Lu Fang, Junjie Bai, and Soumith Chintala. Pytorch: An imperative style, high-performance deep learning library. In *Advances in Neural Information Processing Systems*, pages 8024–8035, 2019.
- Judea Pearl. *Causality*. Cambridge University Press, 2 edition, 2009.
- Judea Pearl. The seven tools of causal inference, with reflections on machine learning. *Communications of the ACM*, 62(3):54–60, feb 2019. ISSN 0001-0782.
- Jonas Peters, Peter Bühlmann, and Nicolai Meinshausen. Causal inference by using invariant prediction: identification and confidence intervals. *Journal of the Royal Statistical Society: Series B (Statistical Methodology)*, 78(5):947–1012, 2016.
- Jonas Peters, Dominik Janzing, and Bernhard Scholkopf. *Elements of Causal Inference: Foundations and Learning Algorithms*. The MIT Press, 2017. ISBN 0262037319.
- Ekagra Ranjan, Soumya Sanyal, and Partha P. Talukdar. ASAP: adaptive structure aware pooling for learning hierarchical graph representations. In *AAAI Conference on Artificial Intelligence*, pages 5470–5477, 2020.
- Mateo Rojas-Carulla, Bernhard Schölkopf, Richard Turner, and Jonas Peters. Invariant models for causal transfer learning. *Journal of Machine Learning Research*, 19(36):1–34, 2018.
- Elan Rosenfeld, Pradeep Kumar Ravikumar, and Andrej Risteski. The risks of invariant risk minimization. In *International Conference on Learning Representations*, 2021.
- Shiori Sagawa*, Pang Wei Koh*, Tatsunori B. Hashimoto, and Percy Liang. Distributionally robust neural networks. In *International Conference on Learning Representations*, 2020.

- Ruslan Salakhutdinov and Geoffrey E. Hinton. Learning a nonlinear embedding by preserving class neighbourhood structure. In *International Conference on Artificial Intelligence and Statistics*, volume 2, pages 412–419, 2007.
- Alvaro Sanchez-Gonzalez, Nicolas Heess, Jost Tobias Springenberg, Josh Merel, Martin A. Riedmiller, Raia Hadsell, and Peter W. Battaglia. Graph networks as learnable physics engines for inference and control. In *International Conference on Machine Learning*, volume 80, pages 4467–4476, 2018.
- Adam Santoro, Felix Hill, David G. T. Barrett, Ari S. Morcos, and Timothy P. Lillicrap. Measuring abstract reasoning in neural networks. In *International Conference on Machine Learning*, volume 80, pages 4477–4486, 2018.
- David Saxton, Edward Grefenstette, Felix Hill, and Pushmeet Kohli. Analysing mathematical reasoning abilities of neural models. In *International Conference on Learning Representations*, 2019.
- Bernhard Schölkopf. Causality for machine learning. *arXiv preprint*, arXiv:1911.10500, 2019.
- Bernhard Schölkopf, Francesco Locatello, Stefan Bauer, Nan Rosemary Ke, Nal Kalchbrenner, Anirudh Goyal, and Yoshua Bengio. Toward causal representation learning. *Proceedings of the IEEE*, 109(5): 612–634, 2021.
- Tom A.B. Snijders and Krzysztof Nowicki. Estimation and prediction for stochastic blockmodels for graphs with latent block structure. In *Journal of Classification*, volume 14, pages 75–100, 1997.
- Richard Socher, Alex Perelygin, Jean Wu, Jason Chuang, Christopher D. Manning, Andrew Y. Ng, and Christopher Potts. Recursive deep models for semantic compositionality over a sentiment treebank. In *Conference on Empirical Methods in Natural Language Processing*, pages 1631–1642, 2013.
- Nitish Srivastava, Geoffrey E. Hinton, Alex Krizhevsky, Ilya Sutskever, and Ruslan Salakhutdinov. Dropout: a simple way to prevent neural networks from overfitting. *Journal of Machine Learning Research*, 15(1):1929–1958, 2014.
- Teague Sterling and John J. Irwin. Zinc 15 – ligand discovery for everyone. *Journal of Chemical Information and Modeling*, 55(11):2324–2337, 2015.
- Hao Tang, Zhiao Huang, Jiayuan Gu, Bao-Liang Lu, and Hao Su. Towards scale-invariant graph-related problem solving by iterative homogeneous gnns. In *Advances in Neural Information Processing Systems*, 2020.
- Naftali Tishby, Fernando C. Pereira, and William Bialek. The information bottleneck method. In *Annual Allerton Conference on Communication, Control and Computing*, pages 368–377, 1999.
- Aäron van den Oord, Yazhe Li, and Oriol Vinyals. Representation learning with contrastive predictive coding. *arXiv preprint*, arXiv:1807.03748, 2018.
- Vladimir Vapnik. Principles of risk minimization for learning theory. In *Advances in Neural Information Processing Systems*, pages 831–838, 1991.
- Petar Veličković, Rex Ying, Matilde Padovano, Raia Hadsell, and Charles Blundell. Neural execution of graph algorithms. In *International Conference on Learning Representations*, 2020.
- Petar Veličković, Guillem Cucurull, Arantxa Casanova, Adriana Romero, Pietro Liò, and Yoshua Bengio. Graph attention networks. In *International Conference on Learning Representations*, 2018.

- Tongzhou Wang and Phillip Isola. Understanding contrastive representation learning through alignment and uniformity on the hypersphere. In *International Conference on Machine Learning*, volume 119, pages 9929–9939, 2020.
- Qitian Wu, Hengrui Zhang, Junchi Yan, and David Wipf. Towards distribution shift of node-level prediction on graphs: An invariance perspective. In *International Conference on Learning Representations*, 2022a.
- Yingxin Wu, Xiang Wang, An Zhang, Xiangnan He, and Tat-Seng Chua. Discovering invariant rationales for graph neural networks. In *International Conference on Learning Representations*, 2022b.
- Louis-Pascal A. C. Xhonneux, Andreea Deac, Petar Veličković, and Jian Tang. How to transfer algorithmic reasoning knowledge to learn new algorithms? In *Advances in Neural Information Processing Systems*, 2021.
- Keyulu Xu, Chengtao Li, Yonglong Tian, Tomohiro Sonobe, Ken-ichi Kawarabayashi, and Stefanie Jegelka. Representation learning on graphs with jumping knowledge networks. In *International Conference on Machine Learning*, pages 5449–5458, 2018.
- Keyulu Xu, Weihua Hu, Jure Leskovec, and Stefanie Jegelka. How powerful are graph neural networks? In *International Conference on Learning Representations*, 2019.
- Keyulu Xu, Jingling Li, Mozhi Zhang, Simon S. Du, Ken-ichi Kawarabayashi, and Stefanie Jegelka. What can neural networks reason about? In *International Conference on Learning Representations*, 2020.
- Keyulu Xu, Mozhi Zhang, Jingling Li, Simon Shaolei Du, Ken-ichi Kawarabayashi, and Stefanie Jegelka. How neural networks extrapolate: From feedforward to graph neural networks. In *International Conference on Learning Representations*, 2021.
- Han Yang, Kaili Ma, and James Cheng. Rethinking graph regularization for graph neural networks. In *AAAI Conference on Artificial Intelligence*, pages 4573–4581, 2021.
- Gilad Yehudai, Ethan Fetaya, Eli Meir, Gal Chechik, and Haggai Maron. From local structures to size generalization in graph neural networks. In *International Conference on Machine Learning*, volume 139, pages 11975–11986, 2021.
- Raymond Yeung. *Information Theory and Network Coding*. 01 2008. ISBN 978-0-387-79233-0.
- Zhitao Ying, Jiaxuan You, Christopher Morris, Xiang Ren, William L. Hamilton, and Jure Leskovec. Hierarchical graph representation learning with differentiable pooling. In *Advances in Neural Information Processing Systems*, pages 4805–4815, 2018.
- Zhitao Ying, Dylan Bourgeois, Jiaxuan You, Marinka Zitnik, and Jure Leskovec. Gnnexplainer: Generating explanations for graph neural networks. In *Advances in Neural Information Processing Systems*, pages 9240–9251, 2019.
- Jiaxuan You, Rex Ying, Xiang Ren, William L. Hamilton, and Jure Leskovec. Graphrnn: Generating realistic graphs with deep auto-regressive models. In *International Conference on Machine Learning*, volume 80, pages 5694–5703, 2018.
- Yuning You, Tianlong Chen, Yongduo Sui, Ting Chen, Zhangyang Wang, and Yang Shen. Graph contrastive learning with augmentations. In *Advances in Neural Information Processing Systems*, volume 33, pages 5812–5823, 2020.

- Yuning You, Tianlong Chen, Yang Shen, and Zhangyang Wang. Graph contrastive learning automated. In *International Conference on Machine Learning*, volume 139, pages 12121–12132, 18–24 Jul 2021.
- Junchi Yu, Tingyang Xu, Yu Rong, Yatao Bian, Junzhou Huang, and Ran He. Graph information bottleneck for subgraph recognition. In *International Conference on Learning Representations*, 2021.
- Hao Yuan, Haiyang Yu, Shurui Gui, and Shuiwang Ji. Explainability in graph neural networks: A taxonomic survey. *arXiv preprint*, arXiv:2012.15445, 2020.
- Yonggang Zhang, Mingming Gong, Tongliang Liu, Gang Niu, Xinmei Tian, Bo Han, Bernhard Schölkopf, and Kun Zhang. Adversarial robustness through the lens of causality. *arXiv preprint*, arXiv:2106.06196, 2021.
- Roland S. Zimmermann, Yash Sharma, Steffen Schneider, Matthias Bethge, and Wieland Brendel. Contrastive learning inverts the data generating process. In *International Conference on Machine Learning*, volume 139, pages 12979–12990, 2021.

Appendix A. More Related Works and Discussions

A.1 More related works

GNN explainability. Works in GNN explanation also aim to find a subgraph of the input as the explanations for the prediction of a GNN model (Ying et al., 2019; Yuan et al., 2020). Though some may leverage causality in explanation generation (Lin et al., 2021), they mostly focus on understanding the predictions of GNNs instead of OOD generalization. Recently there are two works aiming to provide robust explanations against distribution shifts (Chang et al., 2020; Wu et al., 2022b). However, they can hardly be adapted to identify the invariant subgraph for OOD generalization nor provide theoretical guarantees in our circumstances.

GNN extrapolation. Recently there is a surge of attention in improving the extrapolation ability of GNNs and apply them to various applications, such as mathematical reasoning (Santoro et al., 2018; Saxton et al., 2019), physics (Battaglia et al., 2016; Sanchez-Gonzalez et al., 2018), and graph algorithms (Tang et al., 2020; Velickovic et al., 2020; Xu et al., 2020; Xhonneux et al., 2021). Xu et al. (2021) study the neural network extrapolation ability from a geometrical perspective. Knyazev et al. (2019); Yehudai et al. (2021) focus on the extrapolation of GNNs in terms of graph sizes, while making additional assumptions on the knowledge about ground truth attentions and access to test inputs. Bevilacqua et al. (2021) study the graph size extrapolation problem of GNNs through a causal lens, while the induced invariance principle is built upon assumptions on the specific family of graphs. Han et al. (2021) improve OOD drug discovery by mitigating the overconfident misprediction issue. Different from these works, we consider the GNN extrapolation as a causal problem, establish generic SCMs that are compatible with several graph generation models, induce the invariance principle upon SCMs and instantiate it with theoretical guarantees.⁷

Causality and invariant learning. Causality comes to the stage for demystifying and improving the huge success of machine learning algorithms to further advances (Pearl, 2019; Schölkopf, 2019; Schölkopf et al., 2021). One of the most widely applied concept from causality is the Independent Causal Mechanism (ICM) that assumes conditional distribution of each variable given its causes (i.e., its mechanism) does not inform or influence the other conditional distributions (Pearl, 2009; Peters et al., 2017). The invariance principle is also induced from the ICM assumption. Once proper assumptions about the underlying data generation process via Structural Causal Models (SCM) are established, it is promising to apply the invariance principle to machine learning models for finding an invariant representation about the causal relationship between the underlying causes and the label. Consequently, models built upon the invariant representation can generalize to unseen environments or domains with guaranteed performance (Peters et al., 2016; Rojas-Carulla et al., 2018; Arjovsky et al., 2019; Sagawa* et al., 2020; Bengio et al., 2020; Koyama and Yamaguchi, 2020; Gulrajani and Lopez-Paz, 2021; Krueger et al., 2021; Creager et al., 2021; Ahuja et al., 2021). Different from domain adaption or transfer learning (Rojas-Carulla et al., 2018; Chuang et al., 2020) which aims to learn the invariant information shared across source domain and target domain and generically assumes the availability of target domain data, the out of distribution (OOD) generalization problem studied in this paper does not pose such assumptions hence the learned model has to get rid of all spurious correlations introduced via S to be min-max optimal (Eq. 3) and generalize to OOD data with provable guarantees. We refer interested readers to Pearl (2019); Schölkopf (2019); Schölkopf et al. (2021) for in-depth understanding.

A.2 More discussions on connections of GOOD with existing works

Although primarily serving for graph OOD generalization problem, our theory complements the identifiability study on graphs through contrastive learning, and aligns with the discoveries in the image

7. We provide additional details in Appendix C.3.

domain that contrastive learning learns to isolate the content (C) and style (S) (Zimmermann et al., 2021; Kügelgen et al., 2021). Moreover, our theoretical analysis also partially explains the empirical success of graph contrastive learning (You et al., 2020; Ma et al., 2021; You et al., 2021), where the GNN may implicitly learn to identify the underlying invariant subgraph. Besides, the framework of GOOD can also be applied to other tasks involving relational information such as node classification. While we sample positive samples according to the labels, the previous contrastive learning with augmentations can also be applied to Eq. 9 for reducing the sample complexity. supervised contrastive loss in image domain (Khosla et al., 2020).

On expressivity of GOOD. The expressivity of GOOD is essentially constrained by the encoders embedded for learning graph representations. During isolating G_c from G , if the encoder can not differentiate two isomorphic graphs G_c and $G_c \cup G_s^p$ where $G_s^p \subseteq G_s$, then the featurizer will fail to identify the underlying invariant subgraph. Moreover, the classifier will also fail if the encoder can not differentiate two non-isomorphic G_c s from different classes. Thus, adopting more powerful graph representation encoders into GOOD can improve the OOD generalization.

On GOOD and graph information bottleneck. Under the FIIF assumption on latent interaction, the independence condition in Eq. 4 can also be rewritten as $Y \perp\!\!\!\perp S|\hat{\mathcal{G}}_c$, which further implies $Y \perp\!\!\!\perp S|\hat{\mathcal{G}}_c$. Hence it is natural to use Information Bottleneck (IB) objective (Tishby et al., 1999) to solve for G_c :

$$\begin{aligned} \min_{\theta} R_{G_c}(h_{\theta} \circ \rho), \\ \text{s.t. } \mathcal{G}_c = \arg \max_{\hat{\mathcal{G}}_c \subseteq G} I(\hat{\mathcal{G}}_c, Y) - I(\hat{\mathcal{G}}_c, \mathcal{G}), \end{aligned} \quad (11)$$

which explains the success of many existing works in finding predictive subgraph through IB (Yu et al., 2021). However, the estimation of $I(\hat{\mathcal{G}}_c, \mathcal{G})$ is notoriously difficult due to the complexity of graph, which can lead to unstable convergence as observed in our experiments. In contrast, optimization with contrastive objective as Eq. 9 induces smooth and stable convergence. Moreover, Ahuja et al. (2021) introduce IB objective into IRM (Arjovsky et al., 2019) to tackle OOD generalization in linear regime under FIIF assumption, However, it can not be directly applied to our case due to the assumption of Gaussian prior on \mathcal{G}_c for FIIF and the failure of IRM in the non-linear regime (Rosenfeld et al., 2021) for PIIF.

On GOOD for node classification. As the task of node classification can be viewed as graph classification based on the ego-graphs of a node, our analysis and discoveries can generalize to node classification. More specifically, the invariance principle for node classification can be implemented by identifying an invariant subgraph from the K -hop neighbor graph of each node, and making predictions based on it, i.e., $Y \perp\!\!\!\perp E|G_c^{\text{ego}} \subseteq G_u^{\text{ego}}$ for node u (Wu et al., 2022a).

Appendix B. Full Causal Structural Models on Data Generation Process

Assumption B.1 (Graph Generation SCM).

$$\begin{aligned} (Z_A^c, Z_X^c) &:= f_{\text{gen}}^{(A,X)^c}(C), \quad G_c := f_{\text{gen}}^{G_c}(Z_A^c, Z_X^c), \\ (Z_A^s, Z_X^s) &:= f_{\text{gen}}^{(A,X)^s}(S), \quad G_s := f_{\text{gen}}^{G_s}(Z_A^s, Z_X^s, E_G), \\ G &:= f_{\text{gen}}^G(G_c, G_s, E_G). \end{aligned}$$

Assumption B.2 (FIIF SCM).

$$Y := f_{\text{inv}}(C), \quad S := f_{\text{spu}}(C, E), \quad G := f_{\text{gen}}(C, S).$$

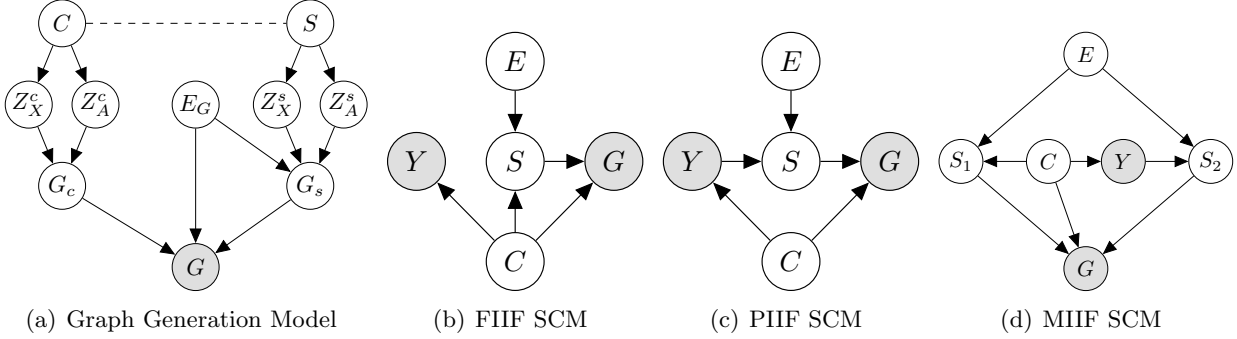


Figure 4: Full SCMs on Graph Distribution Shifts.

Assumption B.3 (PIIF SCM).

$$Y := f_{\text{inv}}(C), S := f_{\text{spu}}(Y, E), G := f_{\text{gen}}(C, S).$$

Assumption B.4 (MIIF SCM).

$$Y := f_{\text{inv}}(C), S_1 := f_{\text{spu}}(C, E), S_2 := f_{\text{spu}}(Y, E), G := f_{\text{gen}}(C, S_1, S_2).$$

Supplementary to the graph generation process in Sec. 3.1, we provide full SCMs on the graph generation process in this section as shown in Fig. 4. Formal descriptions are as Assumptions B.1, B.2, B.3, B.4.

Specifically, the graph generation processes are controlled by $f_{\text{gen}} : \mathcal{Z} \rightarrow \mathcal{G}$. Shown as Fig. 4(a), given the variable partitions C and S at the latent space \mathcal{Z} , they control the generation of the adjacency matrix and features for the invariant subgraph G_c and spurious subgraph G_s through two pairs of latent variables (Z_A^c, Z_X^c) and (Z_A^s, Z_X^s) , respectively. Then, G_c and G_s are entangled into the observed graph G through f_{gen}^G . It can be a simply JOIN of a G_c with one or multiple G_s , or more complex generation processes controlled by the latent variables (Snijders and Nowicki, 1997; Lovász and Szegedy, 2006; You et al., 2018; Luo et al., 2021; Yehudai et al., 2021).

Moreover, a subset of environment latent variable $E_G \subseteq E$ will affect the generation of G and G_s . Thus, graphs collected from different environments can have different structure-level properties such as degrees, graph sizes, homophily, as well as feature-level properties (Knyazev et al., 2019; Yehudai et al., 2021; Bevilacqua et al., 2021; Chen et al., 2022).

As for the interaction between C and S at the latent space, we categorize the interaction modes into Fully Informative Invariant Features (FIIF, Fig. 4(b)), and Partially Informative Invariant Features (PIIF, Fig. 4(c)), depending on whether the latent invariant part C is fully informative about label Y , i.e., $(S, E) \perp\!\!\!\perp Y | C$. It is also possible that FIIF and PIIF are entangled into a Mixed Informative Invariant Features (MIIF, Fig. 4(d)). We follow Arjovsky et al. (2019); Ahuja et al. (2021) to formulate the SCMs for FIIF and PIIF, where we omit noises for simplicity (Pearl, 2009; Peters et al., 2017). Since MIIF is built upon FIIF and PIIF, we will focus on the axiom interaction modes (FIIF and PIIF) in this paper, while most of our discussions can be extended to MIIF or more complex interactions built upon FIIF and PIIF.

Appendix C. More Details about Failure Case Studies in Sec. 3.2

In this section, we provide details on failure case studies in Sec. 3.2. We firstly elaborate the empirical evaluation setting.

C.1 More empirical details about failure case study at Sec. 3.2

We conduct our case studies based on GCN, GIN with mean or sum readout (Kipf and Welling, 2017; Xu et al., 2019), and hidden dimension of 64, optimized with either ERM or IRM (Vapnik, 1991; Arjovsky et al., 2019). As the environment partitions are not available, we generate 2 environments with random partitions. During training, we use a batch size of 32, learning rate of $1e - 3$ with Adam optimizer (Kingma and Ba, 2015), batch normalization between hidden layers (Ioffe and Szegedy, 2015), and early stop the training when the validation accuracy does not increase till 5 epoch after first 20 epochs. All of the experiments are repeated 5 times.

We construct 3-class synthetic datasets based on BAMotif (Luo et al., 2020), where the model needs to tell which motif the graph contains. We inject the distribution shifts in the training data while keep the testing data and validation data without the biases. For structure-level shifts, we introduce the artificial bias based on FIIF, where the motif and the base graph are spuriously correlated with a probability of various bias. For mixed shifts, we additionally introduced attribute-level shifts based on FIIF, where all of the node features are spuriously correlated with a probability of various bias. The number of training graphs is 600 for each class and the number of graphs in validation and testing set is 200 for each class. More construction details are given in Appendix E.

C.2 Theoretical examples for failure case study at Sec. 3.2

Firstly, we follow Ahuja et al. (2021) to introduce the formal examples on the failures of GNNs optimized with ERM or IRM (Vapnik, 1991; Arjovsky et al., 2019) through a linear binary classification problem:

Definition C.1 (Linear classification structural equation model (FIIF)).

$$\begin{aligned} Y &:= (w_{\text{inv}}^* \cdot C) \oplus N, \quad N \sim \text{Ber}(q), \quad N \perp (C, S), \\ X &\leftarrow S(C, S), \end{aligned}$$

where $w_{\text{inv}}^* \in \mathbb{R}^{n_c}$ with $\|w_{\text{inv}}^*\| = 1$ is the labeling hyperplane, $C \in \mathbb{R}^{n_c}$, $S \in \mathbb{R}^{n_s}$ are the corresponding invariant and varying latent variables, N is Bernoulli binary noise with a parameter of q and identical across all environments, \oplus is the XOR operator, S is invertible.

Given data generation process as Assumption B.1, and latent space interaction as Assumption B.2 or B.3, and strictly separable invariant features 3.4, consider a k -layer linearized GNN $h_\theta \circ \rho$ using mean as READOUT for binary graph classification, if $\cup_{e \in \mathcal{E}_{\text{te}}} \text{supp}(\mathbb{P}^e) \not\subseteq \cup_{e \in \mathcal{E}_{\text{tr}}} \text{supp}(\mathbb{P}^e)$:

- (i) For graphs features are generated as Definition C.1, $h_\theta \circ \rho$ optimized with ERM or IRM will fail to generalize OOD (Eq. 3) almost surely;
- (ii) For graphs with more than two nodes, globally same node features generated as Definition C.1, and graph labels that are the same as global node labels, $h_\theta \circ \rho$ optimized with ERM or IRM will fail to generalize OOD (Eq. 3) almost surely;

For graph classification, if the number of nodes is fixed to one, it covers the linear classification as above. When $\cup_{e \in \mathcal{E}_{\text{te}}} \text{supp}(\mathbb{P}^e) \not\subseteq \cup_{e \in \mathcal{E}_{\text{tr}}} \text{supp}(\mathbb{P}^e)$, it implies the S from training environments \mathcal{E}_{tr} does not cover S from testing environments, while C can be covered. Moreover, the condition of strictly separable training data now can be formulated as $\min_{C \in \cup_{e \in \mathcal{E}_{\text{tr}}} (C \subseteq G^e)} \text{sgn}(w_{\text{inv}}^* \cdot C)(w_{\text{inv}}^* \cdot C) > 0$. Recall that ERM trains the model by minimizing the empirical risk (e.g., 0-1 loss) over all training data, and IRM formulates OOD generalization as:

$$\begin{aligned} \min_{\theta, f_c} \frac{1}{|\mathcal{E}_{\text{tr}}|} \sum_{e \in \mathcal{E}_{\text{tr}}} R^e(h_\theta \circ \rho) \\ \text{s.t. } \rho \in \arg \min_{\hat{\rho}} R^e(h_\theta \circ \hat{\rho}), \quad \forall e \in \mathcal{E}_{\text{tr}}. \end{aligned} \tag{12}$$

However, both ERM and IRM can not enable OOD generalization, i.e., finding the ground truth w_{inv}^* , following the Theorem 3 from [Ahuja et al. \(2021\)](#):

Theorem C.2 (Insufficiency of ERM and IRM). *Suppose each $e \in \mathcal{E}_{\text{all}}$ follows Definition. C.1, C are strictly separable, bounded and satisfy the support overlap between \mathcal{E}_{tr} and \mathcal{E}_{te} , and S are bounded, if S does not support the overlap, then both ERM and IRM fail at solving the OOD generalization problem.*

The reason is that, when C from all environments are strictly separable, there can be infinite many Bayes optimal solutions given training data $\{G^e, y^e\}_{e \in \mathcal{E}_{\text{tr}}}$, while there is only one optimal solution that does not rely on S . Hence, the probability of generalization to OOD (finding the optimal solution) tends to be 0 in probability.

As for case (ii), when the GNN uses mean readout to classify more than one node graphs, assuming the graph label is determined by the node label and all of the nodes have the same label that are determined as Definition C.1, then GNN optimized with ERM and IRM will also fail because of the same reasons as case (i).

C.3 Discussions on the failures of previous OOD related solutions

First of all, for IRM or similar objectives ([Sagawa* et al., 2020](#); [Krueger et al., 2021](#); [Ahuja et al., 2021](#); [Bellot and van der Schaar, 2020](#)) that requires environment information or non-trivial data partitions, they can hardly be applied to graphs due to the lack of such information. The reason is that obtaining such information can be expensive due to the abstraction of graphs. Moreover, as proved in Theorem 5.1 of [Rosenfeld et al. \(2021\)](#), when there is not sufficient support overlap between training environments and testing environments, the IRM or similar objectives can fail catastrophically when being applied to non-linear regime. The only OOD objective EIIL ([Creager et al., 2021](#)) that does not require environment labels, also rely on similar assumptions on the support overlap. We also empirically find the failure of it at our experiments.

Moreover, since part of explainability works also try to find a subset of the inputs for interpretable prediction robustly against distribution shifts. Here we also provide a discussion for these works. The first work following this line is InvRAT ([Chang et al., 2020](#)), which develops an information-theoretic objective:

$$\min_{g, f_c} \max_{f_s} R(g \circ f_c, Y) + \lambda h(R(g \circ f_c, Y) - R_e(g \circ f_s, Y, E)). \quad (13)$$

However, it also requires extra environment label for optimization that are often unavailable in graphs. Besides, the corresponding assumption on the data generation for guaranteed performance is essentially PIIF if applied to our case, while it can not provide any theoretical guarantees on FIIF.

We also notice a recent work, DIR ([Wu et al., 2022b](#)) that proposes an alternative objective which does not require environment label:

$$\min \mathbb{E}_s [R(h, Y | \text{do}(S = s))] + \lambda \text{Var}_s (\{R(h, Y | \text{do}(S = s))\}). \quad (14)$$

However, the theoretical justification established for DIR (Theorem 1 to Corollary 1 in [Wu et al. \(2022b\)](#)) essentially depends on quality of the generator g which can be prone to spurious correlations. Thus, DIR can hardly provide any theoretical guarantees when applied to our case.

Appendix D. Theories and Discussions

In this section, we provide proofs for propositions and theorems mentioned in the main paper.

D.1 Proof for Proposition 4.1

Proposition D.1. Let \mathcal{G}_c denote the subgraph space for G_c , given a set of graphs with their labels $\mathcal{D} = \{G^{(i)}, y^{(i)}\}_{i=1}^N$ and \mathcal{E}_{all} that follow the graph generation process in Sec. 3.1 (or Sec. B), a GNN $h \circ \rho : \mathcal{G}_c \rightarrow \mathcal{Y}$ solving the following objective can generalize to OOD graphs in the sense of Definition. 3.5:

$$\min_{\theta} R_{\mathcal{G}_c}(h_{\theta} \circ \rho),$$

where $R_{\mathcal{G}_c}$ is the empirical risk over $\{G_c^{(i)}, y^{(i)}\}_{i=1}^N$ and $G_c^{(i)}$ is the underlying invariant subgraph G_c for $G^{(i)}$.

Proof. We establish the proof with independent causal mechanism (ICM) assumption in SCM (Pearl, 2009; Peters et al., 2017). In particular, given the data generation assumption, i.e., for both FIIF (Assumption 3.2) and PIIF (Assumption 3.3), we have: $\forall e$,

$$\begin{aligned} P(Y|C) &= P(Y|C, E = e) \\ P(Y|G_c) \sum_{G_c} P(G_c|C) &= P(Y|G_c) \sum_{G_c} P(G_c|C, E = e) \\ P(Y|G_c) \sum_{G_c} P(G_c|C) &= P(Y|G_c, E = e) \sum_{G_c} P(G_c|C) \\ P(Y|G_c) &= P(Y|G_c, E = e), \end{aligned} \tag{15}$$

where we call ICM for the first three equalities. From Eq. 15, it suffices to know $P(Y|G_c)$ is invariant across different environments. Hence, a GNN predictor $h \circ \rho : \mathcal{G}_c \rightarrow \mathcal{Y}$ optimized with empirical risk given G_c , essentially minimizing the empirical risk across all environments, i.e., $\min R_{\mathcal{G}_c} = \min \max R^e$. Thus, if $h \circ \rho$ solves $\min R_{\mathcal{G}_c}$, it also solves $\min \max R^e$, hence it elicits a invariant GNN predictor according to Definition. 3.5. \square

D.2 Proof for theorem 4.2 (i)

Theorem D.2 (GOODv1 Induces Invariant GNN). Given a set of graphs with their labels $\mathcal{D} = \{G^{(i)}, y^{(i)}\}_{i=1}^N$ and \mathcal{E}_{all} that follow the graph generation process in Sec. 3.1 with invertible f_{gen}^e and noises set U s.t. $H(U) \rightarrow 0$, assuming that the samples from each training environments with $|\mathcal{E}_{tr}| \geq 2$ are equally distributed, considering a model $g \circ f_c$ induced by GOOD embedded with sufficient expressive permutation invariant encoders $h : \mathcal{G}_c \rightarrow \mathbb{R}^h$ that can differentiate every graph in the support of all environments $\cup_{G^e \in \cup_{e \in \mathcal{E}_{all}} \text{supp}(\mathbb{P}^e)} \mathcal{P}(G^e)$ where $\mathcal{P}(G^e)$ is the power set of G^e : each solution $g \circ f_c$ to the following objective, i.e., the minimizer of Eq. 9, elicits an invariant GNN (Definition. 3.5) that is able to generalize to OOD (Eq. 3) through Proposition 4.1.

$$\max_{g, f_c} I(\hat{G}_c; Y) + I(\hat{G}_c; \tilde{G}_c | Y), \text{ s.t. } |g(G)| \leq r_c, \forall G,$$

where $\hat{G}_c = g(G)$, $\tilde{G}_c = g(\tilde{G})$ and $\tilde{G} \sim P(G|Y)$, i.e., \tilde{G} and G have the same label.

Proof. We re-write the objective as follows:

$$\max_{g, f_c} I(\hat{G}_c; Y) + I(\hat{G}_c; \tilde{G}_c | Y), \text{ s.t. } |g(G)| \leq r_c, \forall G, \tag{16}$$

where $\hat{G}_c = g(G)$, $\tilde{G}_c = g(\tilde{G})$ and $\tilde{G} \sim P(G|Y)$, i.e., \tilde{G} and G have the same label.

The proof of Theorem D.2 is essentially to show the estimated \hat{G}_c through Eq. 16 is the underlying G_c , hence the minimizer of Eq. 16 elicits an invariant GNN predictor, according Proposition D.1. In the next, we are going to take a information-theoretic view of the first term $I(\hat{G}_c; Y)$ and the second term $I(\hat{G}_c; \tilde{G}_c|Y)$ to conclude the proof.

As for the first term, we are going to use the following lemmas:

Lemma D.3. *If all of the environments $e \in \mathcal{E}_{tr}$ are equally distributed, given $|\mathcal{D}_{tr}| = N$ sufficient large, and $R(g \circ f_c) \rightarrow r$ where r is the minimal possible empirical risk, i.e., Bayes optimal, we have:*

$$\frac{1}{N} \sum_{(x_i, y_i) \in \mathcal{D}_{tr}} R(x_i, y_i) = R^e = r, \quad H(\Phi) = H^e(\Phi), \quad \forall e \in \mathcal{E}_{tr}.$$

Given Lemma D.3 and the fact that the empirical risk of $R(g \circ f_c)$ approximates the mutual information $I(\hat{G}_c; Y)$ as an lower bound (Eq. 5, or cf., Alemi et al. (2017); Yu et al. (2021)), when the optimal empirical risk is achieved, it suffices to know the $I(\hat{G}_c; Y)$ is maximized.

Obviously, when $\hat{G}_c = G_c$ is a maximizer of $I(\hat{G}_c; Y) = I(C; Y) = H(Y)$, since $f_{gen}^c : \mathcal{C} \rightarrow \mathcal{G}_c$ is invertible and C causes Y . However, there might be some subset $G_s^p \subseteq G_s$ from the underlying G_s that entail the same information about label, i.e., $I(G_c^l \cup G_s^p; Y) = I(G_c; Y)$ where $\hat{G}_c = G_c^l \cup G_s^p$ and $G_c^l = G_c \cap \hat{G}_c$. For FIIF (Assumption 4(b)), it can not happen otherwise, let $G_c^p = G_c - G_c^l$, then we have:

$$\begin{aligned} I(G_c^l \cup G_s^p; Y) &= I(G_c^l \cup G_c^p; Y) \\ I(G_c^l; Y) + I(G_s^p; Y|G_c^l) &= I(G_c^l; Y) + I(G_c^p; Y|G_c^l) \\ I(G_s^p; Y|G_c^l) &= I(G_c^p; Y|G_c^l) \\ H(Y|G_c^l) - H(Y|G_c^l, G_s^p) &= H(Y|G_c^l) - H(Y|G_c^l, G_c^p) \\ H(Y|G_c^l) - H(Y|G_c^l, G_s^p) &= H(Y|G_c^l), \\ H(Y|G_c^l, G_s^p) &= 0, \end{aligned} \tag{17}$$

where the second last equality is due to $C \rightarrow Y$ and the invertibility of $f_{gen}^c : \mathcal{C} \rightarrow \mathcal{G}_c$ in FIIF. Obviously, it can not hold since knowing G_c^l, G_s^p can not determine Y . While for PIIF, since $S \not\perp\!\!\!\perp Y|C$, it follows $G_s \not\perp\!\!\!\perp Y|G_c$, which means G_s can entail some information about Y other than that entailed by G_c .

To avoid the appearance of spuriously correlated G_s in \hat{G}_c , we will use the second term to eliminate it:

$$\begin{aligned} \max_{g, f_c} I(\hat{G}_c; \tilde{G}_c|Y), \\ = H(\hat{G}_c|Y) - H(\hat{G}_c|\tilde{G}_c, Y), \end{aligned} \tag{18}$$

where $\hat{G}_c = g(G)$, $\tilde{G}_c = g(\tilde{G})$ are two positive samples drawn from the same class (i.e., condition on the same Y). Since the all of the training environments are equally distributed, maximizing $I(\hat{G}_c; \tilde{G}_c|Y)$ is essentially maximizes $I(\hat{G}_c, E = \hat{e}; \tilde{G}_c, E = \tilde{e}|Y)$, $\forall \hat{e}, \tilde{e} \in \mathcal{E}_{tr}$, hence, we have:

$$\begin{aligned} \max_{g, f_c} I(\hat{G}_c; \tilde{G}_c|Y), \\ = I(\hat{G}_c, E = \hat{e}; \tilde{G}_c, E = \tilde{e}|Y) \\ = H(\hat{G}_c, E = \hat{e}|Y) - H(\hat{G}_c, E = \hat{e}|\tilde{G}_c, E = \tilde{e}, Y). \end{aligned} \tag{19}$$

We claim Eq. 19 can eliminate any potential subsets in the estimated \hat{G}_c . Otherwise, suppose there are some subsets $\hat{G}_s^p \subseteq \hat{G}_s$ and $\tilde{G}_s^p \subseteq \tilde{G}_s$ in estimated \hat{G}_c, \tilde{G}_c , where \hat{G}_s, \tilde{G}_s be the corresponding underlying G_s s for \hat{G}_c, \tilde{G}_c . Let \hat{G}_c^* and \tilde{G}_c^* be the ground truth G_c , $\hat{G}_c^p = \hat{G}_c^* - \hat{G}_c$ and $\tilde{G}_c^p = \tilde{G}_c^* - \tilde{G}_c$

be the repelled subsets from corresponding ground truth G_{cs} , and $\hat{G}_c^l = \hat{G}_c^* - \hat{G}_c^p$ and $\tilde{G}_c^l = \tilde{G}_c^* - \tilde{G}_c^p$ be the complement. Recall the constraint that $|G_c| = r_c$, hence if $\hat{G}_c^p \subseteq \hat{G}_c$, then a corresponding \hat{G}_c^p will be repelled from \hat{G}_c .

Note that now $\hat{G}_c = \hat{G}_c^l \cup \hat{G}_c^p$ where $\hat{G}_c^* = \hat{G}_c^p \cup \hat{G}_c^l$. Then, we have:

$$\begin{aligned} H(\hat{G}_c, E = \hat{e}|Y) &= H(E = \hat{e}|\hat{G}_c, Y) + H(\hat{G}_c|E = \hat{e}, Y) \\ &= H(\hat{G}_c^l \cup \hat{G}_c^p|E = \hat{e}, Y) \\ &= H(\hat{G}_c^l|E = \hat{e}, Y) + H(\hat{G}_c^p|\hat{G}_c^l, E = \hat{e}, Y) \end{aligned} \quad (20)$$

where the second equality is due to $E = \hat{e}$ is deterministic. Compared Eq. 20 to that when $\hat{G}_c = \hat{G}_c^*$, we have the entropy change as:

$$\Delta H(\hat{G}_c, E = \hat{e}|Y) = H(\hat{G}_c^p|\hat{G}_c^l, E = \hat{e}, Y) - H(\hat{G}_c^p|\hat{G}_c^l, E = \hat{e}, Y). \quad (21)$$

Since in PIIF, given E and Y , S is determined hence G_s and any subsets of G_s are all determined. Then, it suffices to know that in Eq. 21, $H(\hat{G}_c^p|\hat{G}_c^l, E = \hat{e}, Y) = 0$ while $H(\hat{G}_c^p|\hat{G}_c^l, E = \hat{e}, Y) > 0$ since \hat{G}_c^p can not be determined when given $\hat{G}_c^l, E = \hat{e}, Y$. Thus, when some subset from G_s is included in \hat{G}_c , it will minimize $H(\hat{G}_c, E = \hat{e}|Y)$.

As for $H(\hat{G}_c, E = \hat{e}|\tilde{G}_c, E = \tilde{e}, Y)$, WLOG., we can divide all of the possible cases into two:

- (i) \tilde{G}_c contains some $\tilde{G}_s^p \subseteq \tilde{G}_s$;
- (ii) Both \hat{G}_c and \tilde{G}_c contain some $\hat{G}_s^p \subseteq \hat{G}_s$ and $\tilde{G}_s^p \subseteq \tilde{G}_s$, respectively.

For (i), we have:

$$\begin{aligned} H(\hat{G}_c, E = \hat{e}|\tilde{G}_c, E = \tilde{e}, Y) &= H(\tilde{G}_c^l, \tilde{G}_s^p, E = \hat{e}|\tilde{G}_c, E = \tilde{e}, Y) \\ &= H(\tilde{G}_s^p|\tilde{G}_c^l, E = \tilde{e}, Y, \tilde{G}_c^l, E = \hat{e}) + H(\tilde{G}_c^l, E = \hat{e}|\tilde{G}_c, E = \tilde{e}, Y), \end{aligned} \quad (22)$$

Similarly, in PIIF, given E and Y , S is determined hence G_s and any subset of G_s are all determined. Thus, $H(\tilde{G}_s^p|\tilde{G}_c^l, E = \tilde{e}, Y, \tilde{G}_c^l, E = \hat{e}) = 0$ and we have:

$$\Delta H(\hat{G}_c, E = \hat{e}|\tilde{G}_c, E = \tilde{e}, Y) = -H(\tilde{G}_c^l|\tilde{G}_c, E = \tilde{e}, Y, \tilde{G}_c^l, E = \hat{e}). \quad (23)$$

Furthermore, we have:

$$\begin{aligned} \Delta I(\hat{G}_c, E = \hat{e}; \tilde{G}_c, E = \tilde{e}|Y) &= \Delta H(\hat{G}_c, E = \hat{e}|Y) - \Delta H(\hat{G}_c, E = \hat{e}|\tilde{G}_c, E = \tilde{e}, Y) \\ &= -H(\hat{G}_c^p|\hat{G}_c^l, E = \hat{e}, Y) + H(\tilde{G}_c^p|\tilde{G}_c^l, E = \tilde{e}, Y, \tilde{G}_c^l, E = \hat{e}). \end{aligned} \quad (24)$$

Since conditioning will lower the entropy for both discrete and continuous variables (Cover and Thomas, 2006; Yeung, 2008), we have:

$$\Delta I(\hat{G}_c, E = \hat{e}; \tilde{G}_c, E = \tilde{e}|Y) < 0, \quad (25)$$

which implies the existence of \hat{G}_s^p in \hat{G}_c will lower down the second term in Eq. 16 for the case (i).

For (ii), we have:

$$\begin{aligned} H(\hat{G}_c, E = \hat{e}|\tilde{G}_c, E = \tilde{e}, Y) &= H(\tilde{G}_c^l, \tilde{G}_s^p, E = \hat{e}|\tilde{G}_c^l, \tilde{G}_s^p, E = \tilde{e}, Y) \\ &= H(\hat{G}_s^p|\tilde{G}_c^l, \tilde{G}_s^p, E = \tilde{e}, Y, \tilde{G}_c^l, E = \hat{e}) + H(\tilde{G}_c^l, E = \hat{e}|\tilde{G}_c^l, \tilde{G}_s^p, E = \tilde{e}, Y), \end{aligned} \quad (26)$$

Similarly, $H(\hat{G}_s^p | \tilde{G}_c^l, \tilde{G}_s^p, E = \tilde{e}, Y, \hat{G}_c^l, E = \hat{e}) = 0$ while can not complement the mutual information loss from $\Delta H(\hat{G}_c, E = \hat{e} | Y)$. As for $H(\hat{G}_c^l, E = \hat{e} | \tilde{G}_c^l, \tilde{G}_s^p, E = \tilde{e}, Y)$, as \tilde{G}_s^p is determined given $E = \tilde{e}, Y$,

$$\begin{aligned} H(\hat{G}_c^l, E = \hat{e} | \tilde{G}_c^l, \tilde{G}_s^p, E = \tilde{e}, Y) &= H(\hat{G}_c^l, E = \hat{e} | \tilde{G}_c^l, E = \tilde{e}, Y) \\ &> H(\hat{G}_c^l, E = \hat{e} | \tilde{G}_c^l, \tilde{G}_c^p, E = \tilde{e}, Y), \end{aligned} \quad (27)$$

which will further reduce the $I(\hat{G}_c, E = \hat{e}; \tilde{G}_c, E = \tilde{e} | Y)$ hence can not enable $\Delta I(\hat{G}_c, E = \hat{e}; \tilde{G}_c, E = \tilde{e} | Y) > 0$.

To summarize, only the underlying G_c maximizes the objective (Eq. 16), hence solving for the objective (Eq. 16) can elicit an invariant GNN predictor according to Proposition D.1. \square

D.3 Proof for theorem 4.2 (ii)

Theorem D.4 (GOODv2 Induces Invariant GNN). *Given a set of graphs with their labels $\mathcal{D} = \{G^{(i)}, y^{(i)}\}_{i=1}^N$ and \mathcal{E}_{all} that follow the graph generation process in Sec. 3.1 with invertible f_{gen}^c and noises set U s.t. $H(U) \rightarrow 0$, assuming that the samples from each training environments with $|\mathcal{E}_{tr}| \geq 2$ are equally distributed, considering a model $g \circ f_c$ induced by GOOD embedded with sufficient expressive permutation invariant encoders $h : \mathcal{G}_c \rightarrow \mathbb{R}^h$ that can differentiate every graph in the support of all environments $\cup_{G^e \in \cup_{e \in \mathcal{E}_{all}} \text{supp}(\mathbb{P}^e)} \mathcal{P}(G^e)$ where $\mathcal{P}(G^e)$ is the power set of G^e : each solution $g \circ f_c$ to the following objective, i.e., the minimizer of Eq. 9, elicits an invariant GNN (Definition. 3.5) that is able to generalize to OOD (Eq. 3) through Proposition 4.1.*

$$\begin{aligned} \max_{g, f_c} & I(\hat{G}_c; Y) + I(\hat{G}_c; \tilde{G}_c | Y) + I(\hat{G}_s; Y), \\ \text{s.t.} & I(\hat{G}_s; Y) \leq I(\hat{G}_c; Y), \\ & \hat{G}_s = G - \hat{G}_c, \end{aligned}$$

where $\hat{G}_c = g(G), \tilde{G}_c = g(\tilde{G})$ and $\tilde{G} \sim P(G|Y)$, i.e., \tilde{G} and G have the same label.

Proof. We re-write the objective as follows:

$$\begin{aligned} \max_{g, f_c} & I(\hat{G}_c; Y) + I(\hat{G}_c; \tilde{G}_c | Y) + I(\hat{G}_s; Y), \\ \text{s.t.} & I(\hat{G}_s; Y) \leq I(\hat{G}_c; Y), \\ & \hat{G}_s = G - \hat{G}_c, \end{aligned} \quad (28)$$

where $\hat{G}_c = g(G), \tilde{G}_c = g(\tilde{G})$ and $\tilde{G} \sim P(G|Y)$, i.e., \tilde{G} and G have the same label.

The proof for Theorem D.4 is essentially to show the estimated \hat{G}_c through Eq. 28 is the underlying G_c , hence the minimizer of Eq. 28 elicits an invariant GNN predictor, according Proposition D.1. In the next, we are going to take a information-theoretic view of Eq. 28 separably to conclude the proof.

Lemma D.5. *Given data generation process as Theorem D.4, for both FIIF and PIIF, we have:*

$$I(C; Y) \geq I(S; Y),$$

hence $I(G_c; Y) \geq I(G_s; Y)$.

Proof for Lemma D.5. For both FIIF and PIIF, we have $I(C; Y) = H(Y)$, since C causes Y . For FIIF, since $S \perp\!\!\!\perp Y | C$, we have $I(S; Y | C) = 0$ hence $I(C; Y) = I(C; Y | S) + I(S; Y) \geq I(S; Y)$. For PIIF, we have $I(Y; S) \leq I(Y; Y) = H(Y) = I(C; Y)$. Moreover, since $f_{gen}^c : \mathcal{C} \rightarrow \mathcal{G}_c$ is invertible, $I(G_c; Y) = I(C; Y) \geq I(S; Y) \geq I(G_s; Y)$. \square

Given Lemma D.5, we know \hat{G}_c at least contains some subset of the underlying G_c , otherwise the constraint $I(\hat{G}_s; Y) \leq I(\hat{G}_c; Y)$ will be violated if $G_c \subseteq \hat{G}_s$. Then, consider different \hat{G}_c that:

- (i) contains a subset of the underlying G_c ;
- (ii) contain the underlying G_c as well as part of the underlying G_s ;

If the two scenarios (i) and (ii) can not hold when optimizing Eq. 28, then we can conclude that \hat{G}_c can only contain the underlying G_c .

First of all, for case (i), considering maximizing $I(\hat{G}_c; \tilde{G}_c|Y)$, similar to the proof for Theorem D.2, is essentially maximizing $I(\hat{G}_c, E = \hat{e}; \tilde{G}_c, E = \tilde{e}|Y)$, $\forall \hat{e}, \tilde{e} \in \mathcal{E}_{\text{tr}}$. Since $G_c \perp E$, let \hat{g} be a solution for case (i), if $\exists G_c^p \subseteq G_c$ while $G_c^p \not\subseteq \hat{g}(G)$ for some G , adding the left G_c^p to $\hat{g}(G)$ can always enlarge $I(\hat{G}_c; \tilde{G}_c|Y)$, while not affecting the optimization of $I(\hat{G}_s; Y) + I(\hat{G}_c; Y)$. Thus, case (i) can not hold due to its sub-optimality.

As for case (ii), let \hat{G}_c^* and \tilde{G}_c^* be the ground truth G_c s for \hat{G} and \tilde{G} , \hat{G}_s and \tilde{G}_s be the ground truth G_s s for \hat{G} and \tilde{G} , and $\hat{G}_s^p \subseteq \hat{G}_s$ and $\tilde{G}_s^p \subseteq \tilde{G}_s$ be subsets from G_s s included in estimated \hat{G}_c and \tilde{G}_c , respectively.

Recall that maximizing $I(\hat{G}_c; \tilde{G}_c|Y)$ is essentially maximizing $I(\hat{G}_c, E = \hat{e}; \tilde{G}_c, E = \tilde{e}|Y)$, $\forall \hat{e}, \tilde{e} \in \mathcal{E}_{\text{tr}}$, hence, we have:

$$\begin{aligned} & \max_{g, f_c} I(\hat{G}_c; \tilde{G}_c|Y), \\ & = I(\hat{G}_c, E = \hat{e}; \tilde{G}_c, E = \tilde{e}|Y) \\ & = H(\hat{G}_c, E = \hat{e}|Y) - H(\hat{G}_c, E = \hat{e}|\tilde{G}_c, E = \tilde{e}, Y). \end{aligned} \quad (29)$$

We claim Eq. 29 can eliminate any potential subsets in the estimated \hat{G}_c .

Note that now $\hat{G}_c = \hat{G}_c^* \cup \hat{G}_s^p$ and $\tilde{G}_c = \tilde{G}_c^* \cup \tilde{G}_s^p$. Then, we have:

$$\begin{aligned} H(\hat{G}_c, E = \hat{e}|Y) & = H(E = \hat{e}|\hat{G}_c, Y) + H(\hat{G}_c|E = \hat{e}, Y) \\ & = H(\hat{G}_c^* \cup \hat{G}_s^p|E = \hat{e}, Y) \\ & = H(\hat{G}_c^*|E = \hat{e}, Y) + H(\hat{G}_s^p|\hat{G}_c^*, E = \hat{e}, Y) \\ & = H(\hat{G}_c^*|Y) + H(\hat{G}_s^p|\hat{G}_c^*, E = \hat{e}, Y) \end{aligned} \quad (30)$$

where the second equality is due to $E = \hat{e}$ is deterministic. For both PIIF and FIIF, including additional \hat{G}_s^p in \hat{G}_c can not increase $H(\hat{G}_s^p|\hat{G}_c^*, E = \hat{e}, Y)$ as \hat{G}_s is determined given E, Y in PIIF and E, C in FIIF.

As for $H(\hat{G}_c, E = \hat{e}|\tilde{G}_c, E = \tilde{e}, Y)$, WLOG., we can divide all of the possible cases into two:

- (a) \tilde{G}_c contains some $\tilde{G}_s^p \subseteq \tilde{G}_s$;
- (b) Both \hat{G}_c and \tilde{G}_c contain some $\hat{G}_s^p \subseteq \hat{G}_s$ and $\tilde{G}_s^p \subseteq \tilde{G}_s$, respectively.

For (a), we have:

$$\begin{aligned} H(\hat{G}_c, E = \hat{e}|\tilde{G}_c, E = \tilde{e}, Y) & = H(\tilde{G}_c^*, \tilde{G}_s^p, E = \hat{e}|\tilde{G}_c, E = \tilde{e}, Y) \\ & = H(\tilde{G}_s^p|\tilde{G}_c^*, E = \tilde{e}, Y, \tilde{G}_c^*, E = \hat{e}) + H(\tilde{G}_c^*, E = \hat{e}|\tilde{G}_c, E = \tilde{e}, Y), \end{aligned} \quad (31)$$

Similarly, including additional \hat{G}_s^p in \hat{G}_c brings no benefit for minimizing $H(\hat{G}_c, E = \hat{e}|\tilde{G}_c, E = \tilde{e}, Y)$, as \tilde{G}_s is determined given E, Y in PIIF and E, C in FIIF, i.e., $H(\tilde{G}_s^p|\tilde{G}_c^*, E = \tilde{e}, Y, \tilde{G}_c^*, E = \hat{e}) = 0$.

For (b), we have:

$$\begin{aligned}
H(\hat{G}_c, E = \hat{e} | \tilde{G}_c, E = \tilde{e}, Y) &= H(\tilde{G}_c^*, \tilde{G}_s^p, E = \hat{e} | \tilde{G}_c^*, \tilde{G}_s^p, E = \tilde{e}, Y) \\
&= H(\hat{G}_s^p | \tilde{G}_c^*, \tilde{G}_s^p, E = \tilde{e}, Y, \hat{G}_c^*, E = \hat{e}) + H(\hat{G}_c^*, E = \hat{e} | \tilde{G}_c^*, \tilde{G}_s^p, E = \tilde{e}, Y),
\end{aligned}
\tag{32}$$

Similarly, $H(\hat{G}_s^p | \tilde{G}_c^*, \tilde{G}_s^p, E = \tilde{e}, Y, \hat{G}_c^*, E = \hat{e}) = 0$ as \hat{G}_s is determined given E, Y in PIIF and E, C in FIIF. Moreover, for $H(\hat{G}_c^*, E = \hat{e} | \tilde{G}_c^*, \tilde{G}_s^p, E = \tilde{e}, Y)$, in FIIF, when conditioning on $\tilde{G}_c^*, \tilde{G}_s^p$ can not bring no additional information about \hat{G}_c^* , while in PIIF, when conditioning on Y, \tilde{G}_s^p can not bring no additional information about \hat{G}_c^* either.

To summarize, when maximizing including additional $I(\hat{G}_c; \tilde{G}_c | Y)$, including any additional $G_s^p \subseteq G_s$ can not bring additional benefit while $I(G - \hat{G}_c - G_s^p; Y) \leq I(G - \hat{G}_c; Y)$. Moreover, considering the effects of including G_s^p in \hat{G}_c on the optimization of $I(Y; \hat{G}_c)$, since $G_c \subseteq \hat{G}_c$ and all of the training environments are balanced distributed, maximizing $I(Y; \hat{G}_c)$ essentially maximizes $I(Y; \hat{G}_c | E = e)$, $\forall e \in \mathcal{E}_{\text{tr}}$. For FIIF, including any $G_s^p \subset G_s$ in \hat{G}_c can not contribute to $I(Y; \hat{G}_c | E = e)$, since Y is determined given G_c , while it will decrease $I(G - \hat{G}_c; Y)$. More formally, $\forall G_s^p \subseteq G_s$, we have

$$I(G - \hat{G}_c - G_s^p; Y) \leq I(G - \hat{G}_c; Y), \quad \forall G_s^p \subseteq G_s,$$

while $I(Y; \hat{G}_c | E = e) = I(Y; \hat{G}_c + G_s^p | E = e)$, $\forall e \in \mathcal{E}_{\text{tr}}$. For PIIF, we have:

$$H(Y) = I(Y; \hat{G}_c^*) \geq I(Y; \hat{G}_c) = I(Y; \hat{G}_c^* \cup G_s^p),$$

since Y is determined when given the ground truth G_c .

Hence, only the underlying G_c maximizes the objective (Eq. 28), which implies that solving for the objective (Eq. 28) can elicit an invariant GNN predictor according to Proposition D.1. \square

Appendix E. Detailed Experimental Settings

In this section, we provide more details about our experimental settings in Sec. 5, including the dataset preparation, dataset statistics, baseline and our method implementations as well as evaluation protocols.

Table 4: Information about the datasets used in experiments. The number of nodes and edges are taking average among all graphs. MCC indicates the Matthews correlation coefficient.

Datasets	# Training	# Validation	# Testing	# Classes	# Nodes	# Edges	Metrics
SPMOTIF	9,000	3,000	3,000	3	44.96	65.67	ACC
PROTEINS	511	56	112	2	39.06	145.63	MCC
DD	533	59	118	2	284.32	1,431.32	MCC
NCI1	1,942	215	412	2	29.87	64.6	MCC
NCI109	1,872	207	421	2	29.68	64.26	MCC
SST5	6,090	1,186	2,240	5	19.85	37.70	ACC
TWITTER	3,238	694	1,509	3	21.10	40.20	ACC
CMNIST-SP	40,000	5,000	15,000	2	56.90	373.85	ACC

E.1 Details about the datasets

We provide more details about the motivation and construction method of the datasets that are used in our experiments. Statistics of the datasets are presented in Table 4.

Table 5: Detailed statistics of selected TU datasets. Table from [Yehudai et al. \(2021\)](#); [Bevilacqua et al. \(2021\)](#).

	NCI1			NCI109		
	all	Smallest 50%	Largest 10%	all	Smallest 50%	Largest 10%
Class A	49.95%	62.30%	19.17%	49.62%	62.04%	21.37%
Class B	50.04%	37.69%	80.82%	50.37%	37.95%	78.62%
Num of graphs	4110	2157	412	4127	2079	421
Avg graph size	29	20	61	29	20	61

	PROTEINS			DD		
	all	Smallest 50%	Largest 10%	all	Smallest 50%	Largest 10%
Class A	59.56%	41.97%	90.17%	58.65%	35.47%	79.66%
Class B	40.43%	58.02%	9.82%	41.34%	64.52%	20.33%
Num of graphs	1113	567	112	1178	592	118
Avg graph size	39	15	138	284	144	746

SPMotif datasets. We construct 3-class synthetic datasets based on BAMotif ([Ying et al., 2019](#); [Luo et al., 2020](#); [Wu et al., 2022b](#)), where the model needs to tell which one of three motifs (House, Cycle, Crane) that the graph contains. For each dataset, we generate 3000 graphs for each class at the training set, 1000 graphs for each class at the validation set and testing set, respectively. During the construction, we merely inject the distribution shifts in the training data while keep the testing data and validation data without the biases. For structure-level shifts (**SPMotif-Struc**), we introduce the bias based on FIIF, where the motif and one of the three base graphs (Tree, Ladder, Wheel) are artificially (spuriously) correlated with a probability of various biases, and equally correlated with the other two. Specifically, given a predefined bias b , the probability of a specific motif (e.g., House) and a specific base graph (Tree) will co-occur is b while for the others is $(1 - b)/2$ (e.g., House-Ladder, House-Wheel). We use random node features for SPMotif-Struc, in order to study the influences of structure level shifts. Moreover, to simulate more realistic scenarios where both structure level and topology level have distribution shifts, we also construct **SPMotif-Mixed** for mixed distribution shifts. We additionally introduced FIIF attribute-level shifts based on SPMotif-Struc, where all of the node features are spuriously correlated with a probability of various biases by setting to the same number of corresponding labels. Specifically, given a predefined bias b , the probability that all of the node features of a graph has label y (e.g., $y = 0$) being set to y (e.g., $\mathbf{X} = \mathbf{0}$) is b while for the others is $(1 - b)/2$ (e.g., $P(\mathbf{X} = \mathbf{1}) = P(\mathbf{X} = \mathbf{2}) = (1 - b)/2$). More complex distribution shift mixes can be studied following our construction approach, which we will leave for future works.

TU datasets. To study the effects of graph sizes shifts, we follow [Yehudai et al. \(2021\)](#); [Bevilacqua et al. \(2021\)](#) to study the OOD generalization abilities of various methods on four of TU datasets ([Morris et al., 2020](#)), i.e., **PROTEINS**, **DD**, **NCI1**, **NCI109**. Specifically, we use the data splits generated by [Yehudai et al. \(2021\)](#) and use the Matthews correlation coefficient as evaluation metric following [Bevilacqua et al. \(2021\)](#) due to the class imbalance in the splits. The splits are generated as follows: Graphs with sizes smaller than the 50-th percentile are assigned to training, while graphs with sizes larger than the 90-th percentile are assigned to test. A validation set for hyperparameters tuning consists of 10% held out examples from training. We also provide a detailed statistics about these datasets in table 5.

Graph-SST datasets. Inspired by the data splits generation for studying distribution shifts on graph sizes, we split the data curated from sentiment graph data ([Yuan et al., 2020](#)), that converts

sentiment sentence classification datasets **SST5** and **SST-Twitter** (Socher et al., 2013; Dong et al., 2014) into graphs, where node features are generated using BERT (Devlin et al., 2019) and the edges are parsed by a Biaffine parser (Gardner et al., 2018). Our splits are created according to the averaged degrees of each graph. Specifically, we assign the graphs as follows: Those that have smaller or equal than 50-th percentile averaged degree are assigned into training, those that have averaged degree large than 50-th percentile while smaller than 80-th percentile are assigned to validation set, and the left are assigned to test set. For SST5 we follow the above process while for Twitter we conduct the above split in an inversed order to study the OOD generalization ability of GNNs trained on large degree graphs to small degree graphs.

CMNIST-sp. To study the effects of PIIF shifts, we select the ColoredMnist dataset created in IRM (Arjovsky et al., 2019). We convert the ColoredMnist into graphs using super pixel algorithm introduced by Knyazev et al. (2019). Specifically, the original Mnist dataset are assigned to binary labels where images with digits 0 – 4 are assigned to $y = 0$ and those with digits 5 – 9 are assigned to $y = 1$. Then, y will be flipped with a probability of 0.25. Thirdly, green and red colors will be respectively assigned to images with labels 0 and 1 an averaged probability of 0.15 (since we do not have environment splits) for the training data. While for the validation and testing data the probability is flipped to 0.9.

E.2 Implementations of GOOD introduced in Sec. 4

Note that GOOD can have multiple implementations. For the purpose of verifying our theory, we do not choose sophisticated architectures in our experiments. Experimental results in Sec. 5 also demonstrates the promising OOD generalization ability of GOOD is general with basic GNN architecture hence can be easily integrated into the existing works from the prosperous GNN literature.

We now introduce the details of the architectures used in our experiments. Recall that GOOD decomposes a model for graph classification into two modules, i.e., a featurizer: $g : \mathcal{G} \rightarrow \mathcal{G}_c$ and a classifier $f_c : \mathcal{G}_c \rightarrow \mathcal{Y}$. Specifically, for the implementation of Featurizer, we choose one of the common practices GAE (Kipf and Welling, 2016) for calculating the sampled weights for each edge. More formally, the soft mask is predicted through the following equation:

$$Z = \text{GNN}(G) \in \mathbb{R}^{n \times h}, M = \sigma(ZZ^T) \in \mathbb{R}^{n \times n}.$$

If a sampling ratio r_c is predetermined, we sample r_c of total edges with the largest predicted weights as a soft estimation of \hat{G}_c . Then, the estimated \hat{G}_c will be forwarded to the classifier f_c for predicting the labels of the original graph. Though Theorem D.2 assumes r_c is known, in real applications we do not know the specific r_c . Hence, in experiments, we select r_c according to the validation performance. To thoroughly study the effects of $I(\hat{G}_s; Y)$ comparing to GOODv1, we stick to using the same r_c and sampling process for GOODv2, while GOODv2 essentially requires less specific knowledge about ground truth r_c hence achieving better empirical performance.

For the implementation of the information theoretic objectives, we will elaborate the GOODv2 while the implementation of GOODv1 can be obtained via removing the third term from GOODv2. Recall that GOODv2 has the following formulation:

$$\begin{aligned} \max_{g, f_c} & I(\hat{G}_c; Y) + I(\hat{G}_c; \tilde{G}_c | Y) + I(\hat{G}_s; Y), \\ \text{s.t.} & I(\hat{G}_s; Y) \leq I(\hat{G}_c; Y), \\ & \hat{G}_s = G - \hat{G}_c, \end{aligned} \tag{33}$$

where $\hat{G}_c = g(G)$, $\tilde{G}_c = g(\tilde{G})$ and $\tilde{G} \sim P(G|Y)$, i.e., \tilde{G} and G have the same label. In Sec. 4.3, we

introduce a contrastive approximation for $I(\hat{G}_c; \tilde{G}_c|Y)$:

$$I(\hat{G}_c; \tilde{G}_c|Y) \approx \mathbb{E}_{\substack{(\hat{G}, \tilde{G}) \sim \mathcal{P}(\hat{G}, \tilde{G}|y) \\ \{G^i\}_{i=1}^M \sim \mathcal{P}(G|Y \setminus y)}} \sigma(\hat{G}, \tilde{G}, \{G^i\}_{i=1}^M), \quad (34)$$

where $\sigma(\hat{G}, \tilde{G}, \{G^i\}_{i=1}^M)$ is defined as:

$$\sigma(\hat{G}, \tilde{G}, \{G^i\}_{i=1}^M) = \log \frac{e^{\phi(h_{\hat{G}_c}, h_{\tilde{G}_c})}}{e^{\phi(h_{\hat{G}_c}, h_{\tilde{G}_c})} + \sum_i^M e^{\phi(h_{\hat{G}_c}^T, h_{G_c^i})}},$$

where ϕ represents a similarity metric, e.g., cosine similarity, and $\hat{G}_c = g(\hat{G})$, $\tilde{G}_c = g(\tilde{G})$, $G_c^i = g(G^i)$. As $|M| \rightarrow \infty$, Eq. 34 approximates $I(\hat{G}_c; \tilde{G}_c|Y)$ in the sense of non-parametric resubstitution entropy estimator via von Mises-Fisher kernel density estimation (Ahmad and Lin, 1976; Kandasamy et al., 2015; Wang and Isola, 2020).

While for the third term $I(\hat{G}_s; Y)$ and the constraint $I(\hat{G}_s; Y) \leq I(\hat{G}_c; Y)$, a straightforward implementation is to imitate the hinge loss:

$$I(\hat{G}_s; Y) \sim \frac{1}{N} R_{\hat{G}_s} \cdot \mathbb{I}(R_{\hat{G}_s} \leq R_{\hat{G}_c}), \quad (35)$$

where N is the number of samples, \mathbb{I} is a indicator function that outputs 1 when the interior condition is satisfied otherwise 0, and $R_{\hat{G}_s}$ and $R_{\hat{G}_c}$ are the empirical risk vector of the predictions for each sample based on G_s and G_c respectively. One can also formulate Eq. 33 from game-theoretic perspective (Chang et al., 2020).

Finally, we can derive the specific loss for the optimization of GOODv2 combining Eq. 34 and Eq. 35:

$$\begin{aligned} & R_{\hat{G}_c} + \alpha \mathbb{E}_{\substack{(\hat{G}, \tilde{G}) \sim \mathcal{P}(\hat{G}, \tilde{G}|y) \\ \{G^i\}_{i=1}^M \sim \mathcal{P}(G|Y \setminus y)}} \log \frac{e^{\phi(h_{\hat{G}_c}, h_{\tilde{G}_c})}}{e^{\phi(h_{\hat{G}_c}, h_{\tilde{G}_c})} + \sum_i^M e^{\phi(h_{\hat{G}_c}^T, h_{G_c^i})}} \\ & + \beta \frac{1}{N} R_{\hat{G}_s} \cdot \mathbb{I}(R_{\hat{G}_s} \leq R_{\hat{G}_c}), \end{aligned} \quad (36)$$

where $R_{\hat{G}_c}, R_{\hat{G}_s}$ are the empirical risk when using \hat{G}_c, \hat{G}_s to predict Y through the classifier, $h_{\hat{G}_c}$ is the permutation invariant representation of \hat{G}_c which can be induced from the GNN encoder either in the featurizer or in the classifier, α, β are the weights for $I(\hat{G}_c; \tilde{G}_c|Y)$ and $I(\hat{G}_s; Y)$, and ϕ is implemented as cosine similarity. The optimization loss for GOODv1 merely contains the first two terms in Eq. 36.

The detailed algorithm for GOOD is given in the following Algorithm, assuming the $h_{\hat{G}_c}$ is obtained via the graph encoder in f_c .

E.3 Training and Optimization in Experiments

For fair comparison, GOOD uses the same GNN architecture for GNN encoders as the baseline methods, whereas α is taken from $\{0.5, 1, 2, 4, 8, 16\}$ and β is taken from $\{0.5, 1, 2, 4\}$ according to the validation performances. Moreover, we also have various options for obtaining the features in \hat{G}_c , for obtaining $h_{\hat{G}_c}$, as well as for obtaining predictions based on \hat{G}_s . Options for obtaining the features in \hat{G}_c are: {from g , from the raw features}. Options for obtaining $h_{\hat{G}_c}$ are: {from the GNN encoder of the classifier f_c with the same pooling as the classifier, from the GNN encoder of the featurizer g with a SUM global pooling, }. Options for obtaining predictions based on \hat{G}_s are: {from another classifier with shared GNN encoder of f_c , from another classifier with shared GNN encoder of f_c while without gradients backwards to the encoder, from a single GNN convolution and a same pooling as f_c }. We

Algorithm 1 Pseudo code for GOOD framework.

Input: Training graphs and labels $\mathcal{D}_{\text{tr}} = \{G_i, y_i\}_{i=1}^N$; learning rate l ; loss weights α, β required for Eq. 36; training epochs e ; batch size b ;
Randomly initialize parameters of g, f_c ;
for $i = 1$ **to** e **do**
 Sample a batch of graphs $\{G^j, y^j\}_{j=1}^b$;
 Estimate the invariant subgraph for the batch: $\{\hat{G}_c^j\}_{j=1}^b = g(\{G^j, y^j\}_{j=1}^b)$;
 Make predictions based the estimated invariant subgraph: $\{\hat{y}^j\}_{j=1}^b = f_c(\{\hat{G}_c^j\}_{j=1}^b)$;
 Calculate the empirical loss $R_{\hat{G}_c}$ with $\{\hat{y}^j\}_{j=1}^b$;
 Fetch the graph representations from f_c as $\{h_{\hat{G}_c}^j\}_{j=1}^b$;
 Calculate the contrastive loss R_c with Eq. 34, where positive samples and negative samples are constructed from the batch;
 Obtain \hat{G}_s the invariant subgraph for the batch: $\{\hat{G}_s^j\}_{j=1}^b = \{G^j - \hat{G}_c^j\}_{j=1}^b$;
 Make predictions based the \hat{G}_s : $\{\hat{y}_s^j\}_{j=1}^b = f_c(\{\hat{G}_s^j\}_{j=1}^b)$;
 Calculate the empirical loss $R_{\hat{G}_s}$ with $\{\hat{y}_s^j\}_{j=1}^b$, and weighted as Eq. 35, as R_s ;
 Updated parameters of g, f_c with respect to $R_{\hat{G}_c} + \alpha R_c + \beta R_s$;
end for

select the corresponding options according to the validation performance with several runs of random α and β , and stick to one for each dataset. As a result, we empirically find using the raw node features for \hat{G}_c , obtaining $h_{\hat{G}_c}$ via a global ADD pooling with the featurizer outputs, and obtaining predictions based on \hat{G}_s from another classifier with shared GNN encoder of f_c while without gradients backwards to the encoder, has better validation performances. Except for TU datasets where we use the outputs of g as the features of \hat{G}_c , and obtain predictions with one GNN layer for the prediction of \hat{G}_s empirically has better validation performances.

Moreover, as a byproduct of this paper, we will keep updating more empirical results with more architectures, formulations of Eq. 33 as well as representation options as above, serving for benchmarking different GNN architectures and fully realization of the power of GOOD in terms of OOD generalization performances on graphs.

Full codes will be made publicly available upon acceptance.

E.4 Implementations of baselines

We elaborate the details for our implementations of baselines in this section. Specifically, for GIB (Yu et al., 2021) and ASAP (Ranjan et al., 2020) we also use the author released codes, and for ASAP (Ranjan et al., 2020). During the implementation, we use the same r_c for both GIB and ASAP. However, we empirically observe that the optimization process in GIB can be unstable during its nested optimization for approximating of the mutual information of the predicted subgraph and the input graph. We use a larger batch size of 128 or reduce the nested optimization steps to be lower than 20 for stabilizing the performance. If the optimization failed due to the instability during training, we will select the results with best validation accuracy as the final outcomes. For ASAP, similar phenomenon is also observed during the experiment for NCI1 dataset due to the choice of r_c , where we set the r_c to 0.7 for ASAP specifically while for others it is 0.6. For DIR (Wu et al., 2022b), we use the codes provided by the authors⁸. We select the hyperparamter for the proposed DIR regularization from

8. <https://anonymous.4open.science/r/DIR/>

$\{0.01, 0.1, 1, 10\}$ according to the validation performances at the datasets, while we stick to the authors claimed hyperparameters for the datasets they also experimented with.

Besides, we refer the implementations in DomainBed (Gulrajani and Lopez-Paz, 2021) for IRM (Arjovsky et al., 2019), V-Rex (Krueger et al., 2021) and IB-IRM (Ahuja et al., 2021). For EIIL (Creager et al., 2021), we use the author released implementations about assigning different samples the weights for being put in each environment and calculating the IRM loss. Since the environment information is not available, we perform random partitions on the training data to obtain two equally large environments for these objectives. Moreover, we select the weights for the corresponding regularization from $\{0.01, 0.1, 1, 10, 100\}$ for these objectives according to the validation performances of IRM and stick to it for others, since we empirically observe that they perform similarly with respect to the regularization weight choice.

E.5 Evaluation and optimization details

During the experiments, we do not turn the hyperparameters exhaustively while following the common recipes for optimizing GNNs. By default, we use Adam optimizer (Kingma and Ba, 2015) with a learning rate of $1e-3$ and a batch size of 32 for all models at all datasets. All GNNs in our experiments have 3 layers and Batch Normalization (Ioffe and Szegedy, 2015), where the hidden dimensions are chose from $\{32, 64, 128\}$ and finalized to 32, 32, 64, 32, 128, 128 for SPMotif, Proteins and DD and NCI1, NCI109, CMNIST, SST5, and Twitter. Experiments in Sec. 5 use the GCN with mean readout (Kipf and Welling, 2017) by default for all datasets except Proteins where we empirically observe better validation performance with a GIN and max readout (Xu et al., 2019). We also employ an early stopping of 5 epochs according the validation performance, after 20, 20, 5, 10, 5 training epochs for SPMotif, TU datasets, CMnist, SST5, and Twitter, in order to prevent overfitting. We also use dropout (Srivastava et al., 2014) with a dropout rate of 0.5 for CMNIST, SST5, Twitter, and 0.3 for TU datasets following the practice of Bevilacqua et al. (2021). For the choice of r_c we search it from $\{0.1, 0.2, 0.25, 0.3, 0.4, 0.5, 0.6, 0.7, 0.8, 0.9\}$ according to the validation performances and set to 0.25, 0.3, 0.6, 0.7, 0.8, 0.5 for SPMotif, Proteins and DD, NCI1, NCI109, CMnist, SST5 and Twitter, respectively. We run each experiment 10 on TU datasets and 5 times for others, and report the mean and standard deviation of the corresponding metrics.

E.6 Software and hardware

We implement our methods with PyTorch (Paszke et al., 2019) and PyTorch Geometric (Fey and Lenssen, 2019). We ran our experiments on Linux Servers with 40 cores Intel(R) Xeon(R) Silver 4114 CPU @ 2.20GHz, 256 GB Memory, and Ubuntu 18.04 LTS installed. GPU environments are varied from 4 NVIDIA RTX 2080Ti graphics cards with CUDA 10.2, 2 NVIDIA RTX 2080Ti and 2 NVIDIA RTX 3090Ti graphics cards with CUDA 11.3, and NVIDIA TITAN series with CUDA 11.3.